X-ray polarimetry with the Gas Pixel Detector

Paolo Soffitta, Enrico Costa, Sergio Fabiani, Fabio Muleri, Alda Rubini
IAPS/INAF Rome
Ronaldo Bellazzini, Alessandro Brez, Massimo Minuti,
Michele Pinchera, Gloria Spandre
INFN-Pisa Italy

Photoelectric effect

Polarimetry based on photoelectric effect was tempted very long ago but it is now a mature technology.

Heitler W.,The Quantum Theory of Radiation

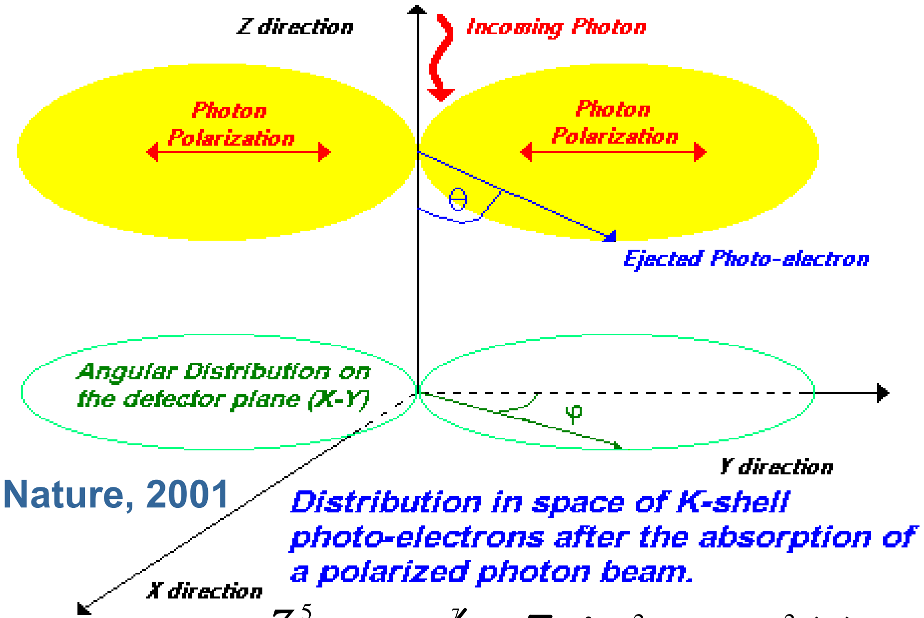

Costa, Nature, 2001

$\beta = v/c$

$$— \quad r_o^2 \frac{Z^5}{137^4} \frac{mc^2}{h}^{7/2} \frac{4\sqrt{2}\,\sin^2 \quad \cos^2(\ )}{(1 \quad \cos \quad)^4}$$

By measuring the angular distribution of the ejected photoelectrons (the modulation curve) it is possible to derive the X-ray polarization.

An X-ray photon directed along the Z axis with the electric vector along the Y axis, is absorbed by an atom.

The photoelectron is ejected at an angle θ (the polar angle) with respect the incident photon direction and at an azimuthal angle φ with respect to the electric vector.

If the ejected electron is in 's' state (as for the K–shell) the differential cross section depends on $\cos^2(\varphi)$, therefore it is preferentially emitted in the direction of the electric field.

Being the cross section always null for φ = 90° the modulation factor μ equals 1 for any polar angle.

X-ray polarimetry with a Gas Pixel Detector

A photon cross a Beryllium window and it is absorbed in the gas gap, the photoelectron produces a track. The track drifts toward the multiplication stage that is the GEM (Gas Electron Multiplier) which is a kapton foil metallized on both side and perforated by microscopic holes (30 um diameter, 50 um pitch) and it is then collected by the pixellated anode plane that is the upper layer of an ASIC chip.

1-cm drift, 1-bar.
He-DME (20-80) 2-10 keV.

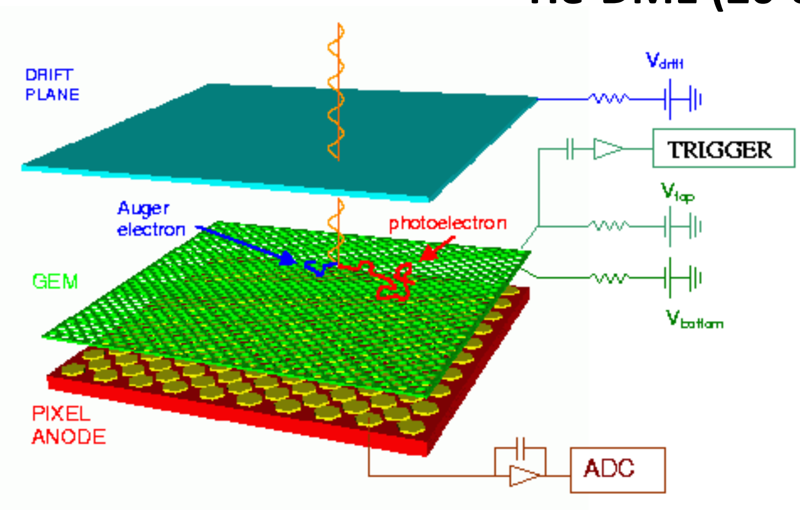

Costa et al., 2001, Bellazzini et al.2006, 2007

GEM electric field

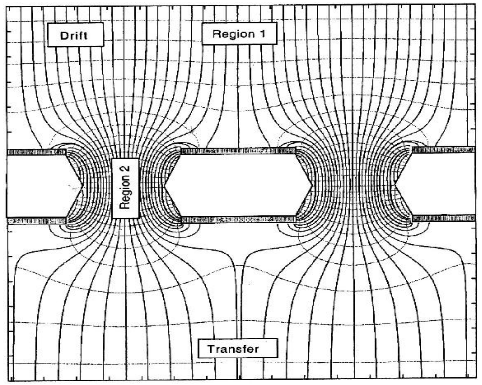

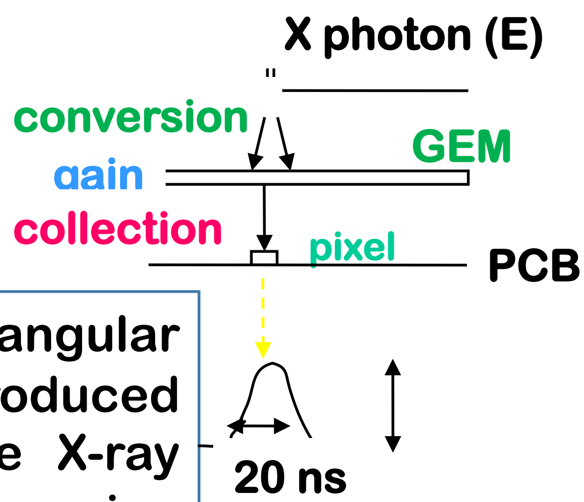

Polarization information is derived from the angular distribution of the emission direction of the tracks produced by the photoelectrons that brings memory of the X-ray polarization. The detector has a very good imaging capability.

ASIC features 105600 pixels 50 μm pitch

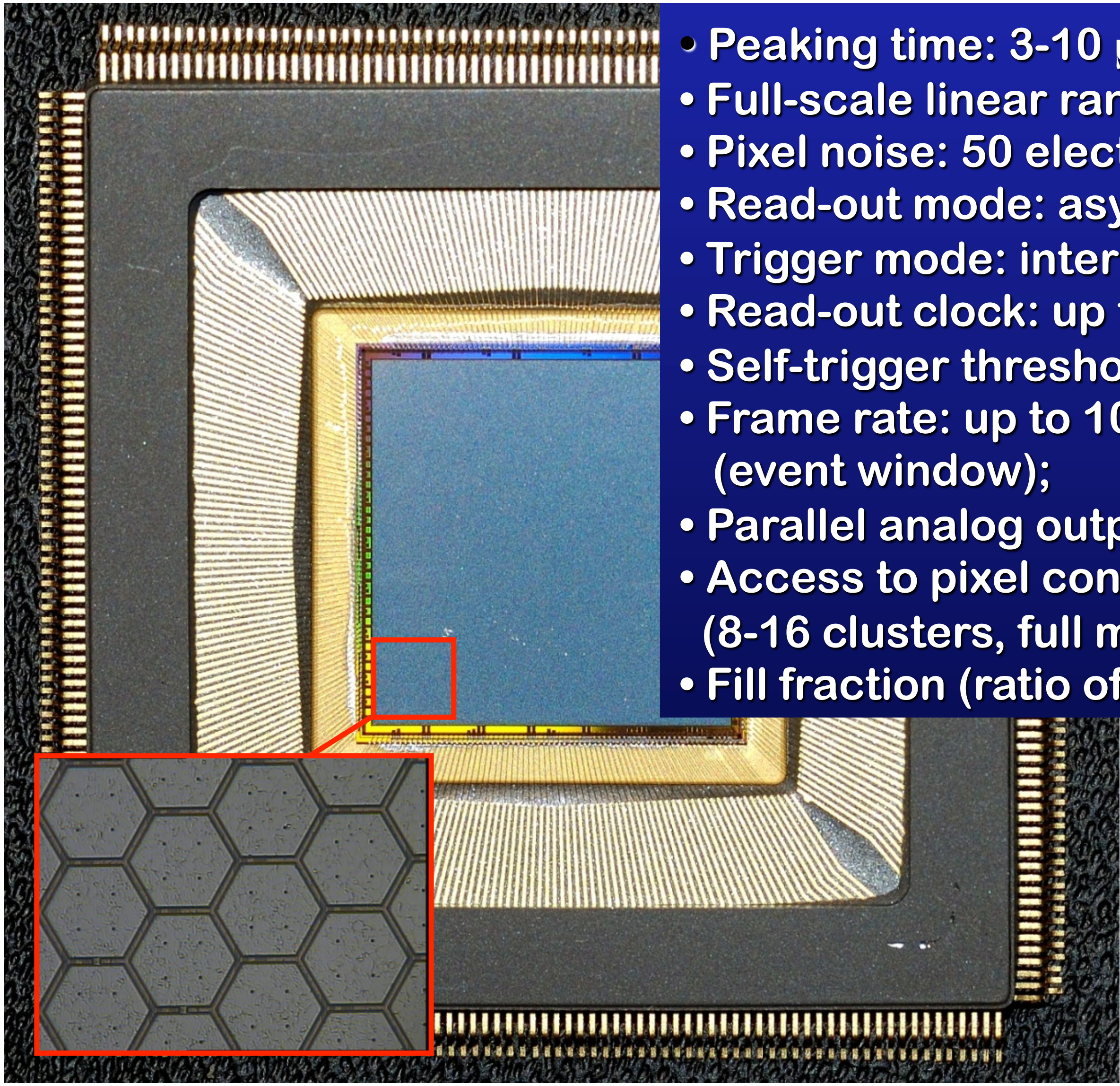

- Peaking time: 3-10 μs, externally adjustable;
- Full-scale linear range: 30000 electrons;
- Pixel noise: 50 electrons ENC;
- Read-out mode: asynchronous or synchronous;
- Trigger mode: internal, external or self-trigger;
- Read-out clock: up to 10MHz;
- Self-trigger threshold: 2200 electrons (10% FS);
- Frame rate: up to 10 kHz in self-trigger mode (event window);
- Parallel analog output buffers: 1, 8 or 16;
- Access to pixel content: direct (single pixel) or serial (8-16 clusters, full matrix, region of interest);
- Fill fraction (ratio of metal area to active area): 92%)

The chip is self-triggered and low noise. The top layer is the collection plane. The bottom 4 layers are a complete analogue chain for each pixel with preamplifier/shaper/sample and hold and serial readout.

It defines the sub-frame that surrounds the track. The dead time downloading an average of 1000 pixels is 100 time lower than for 1E5 pixels.

A new prototype with an extended GEM for better drift field uniformity

Mixture filling	He 20% + DME 80% 1 bar
Gas cell thickness	1 cm
GEM	50 um pitch, 50 um thick, 88 x 88 mm

NEW

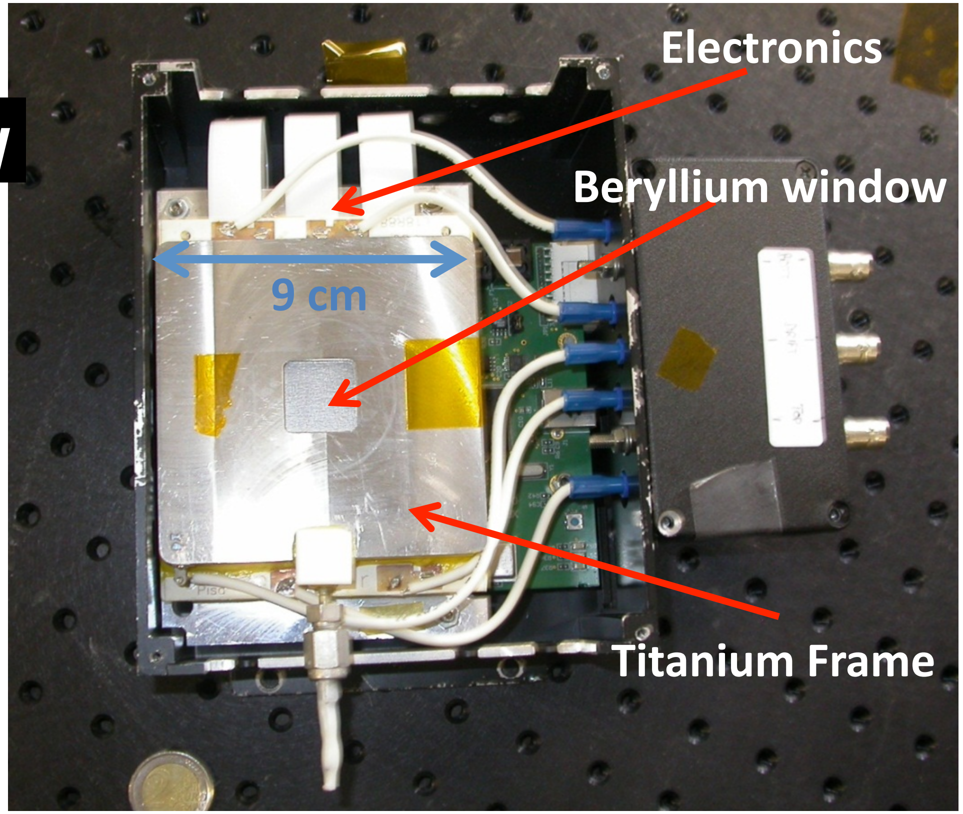

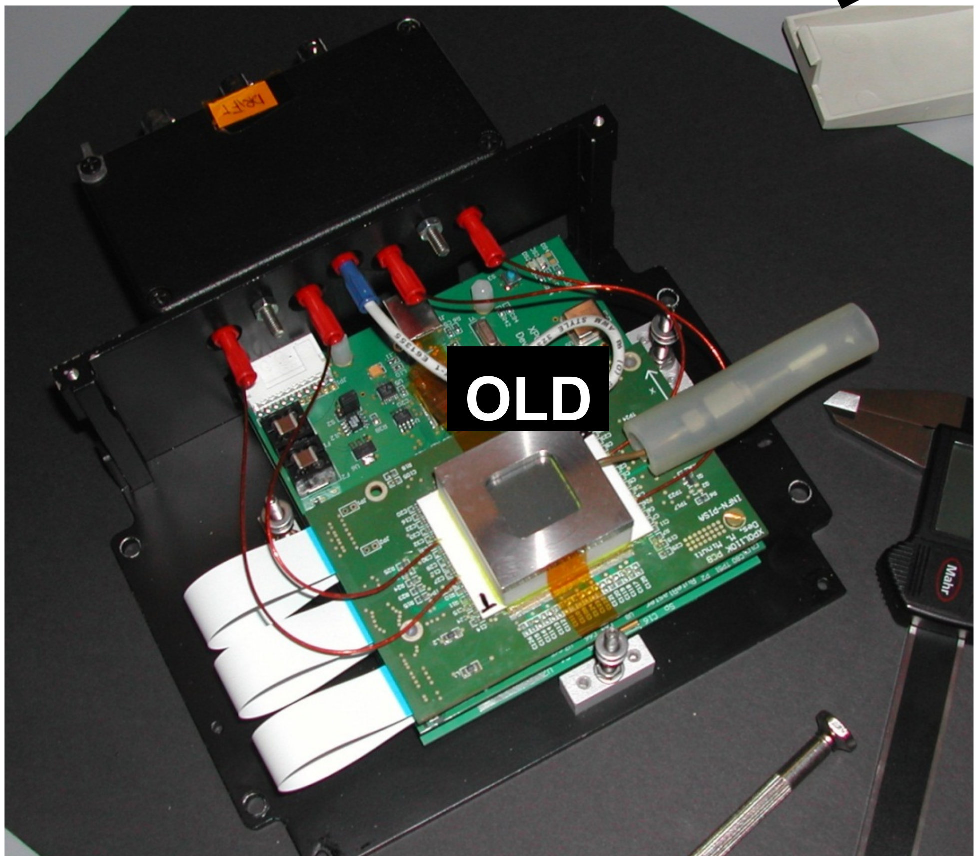

400 g detector, 1.4 kg electronics and box
5 W power consumption

Same window, same ASIC with a larger GEM plane (larger guard ring).

Tracks analysis

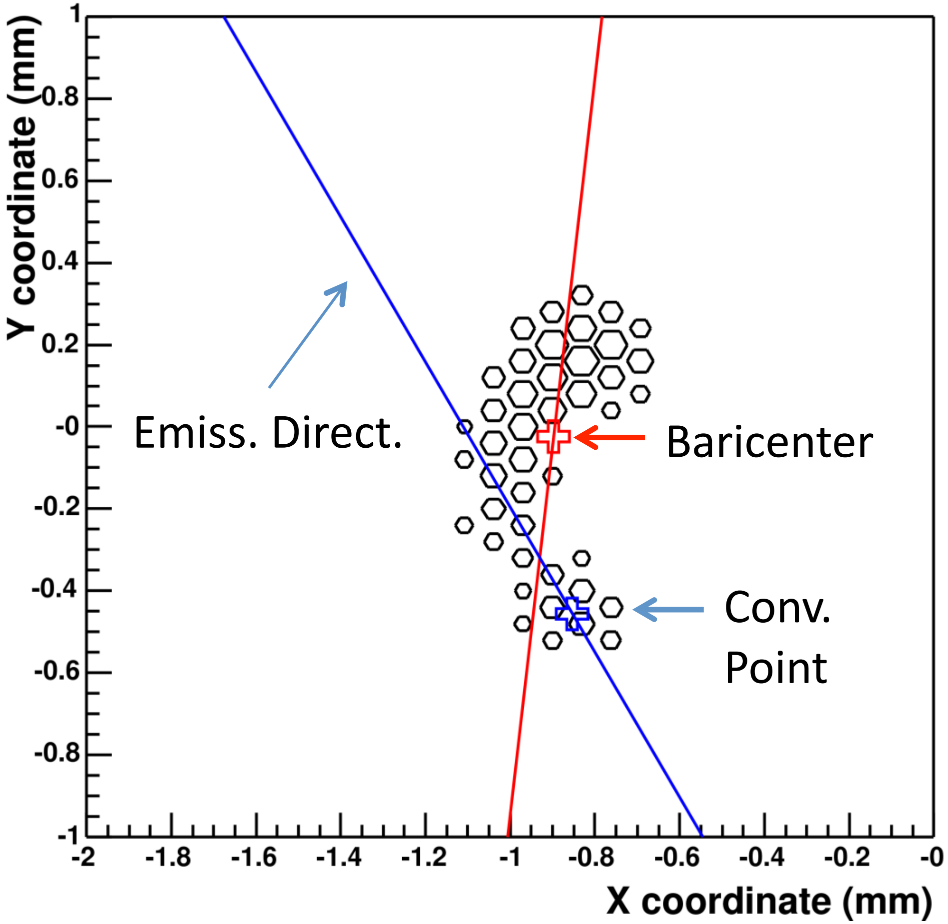

1) **The track is collected by the ASIC**

2) **Baricenter evaluation (using all the triggered pixels)**

3) Reconstruction of the principal axis of the track: maximization of the second moment of charge distribution

4) Reconstruction of the conversion point: third moment along the principal axis (asymmetry of charge distribution to select the lower density end) + second moment (length) to select the region for conversion point determination).

5)Reconstruction of emission direction: (maximization of the second moment with respect to the conversion point) but with pixels weighted according to the distance from it.

From the analysis of the track we reconstruct the original direction of the photoelectron (blue line) and the impact point (blue cross).

IAPS-Rome facility for the production of polarized X-rays.

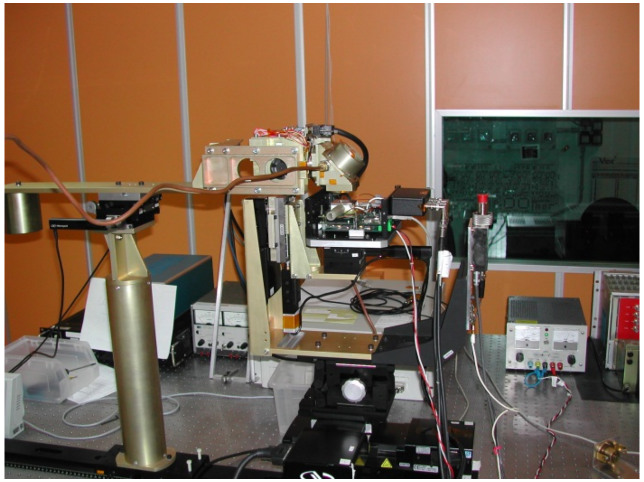

Facility at IASF-Rome/INAF

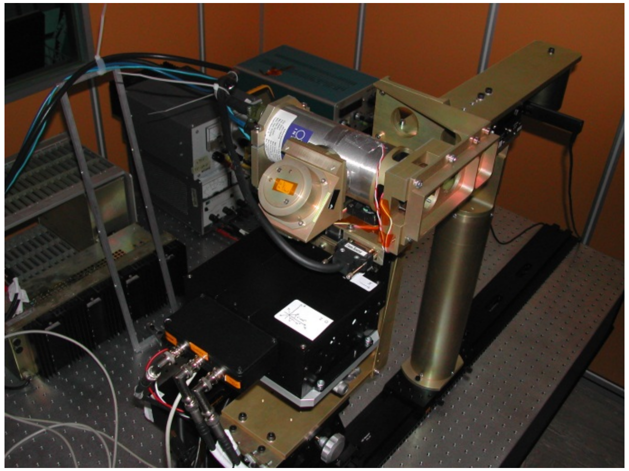

Close-up view of the polarizer and the Gas Pixel Detector

keV	Crystal	Line	Bragg angle
1.65	ADP(101)	CONT	45.0
2.01	PET(002)	CONT	45.0
2.29	Rh(001)	Mo L_α	45.3
2.61	Graphite	CONT	45.0
3.7	Al(111)	Ca K_α	45.9
4.5	CaF_2(220)	Ti K_α	45.4
5.9	LiF(002)	^{55}Fe	47.6
8.05	Ge(333)	Cu K_α	45.0
9.7	FLi(420)	Au L_α	45.1
17.4	Fli(800)	Mo K_α	44.8

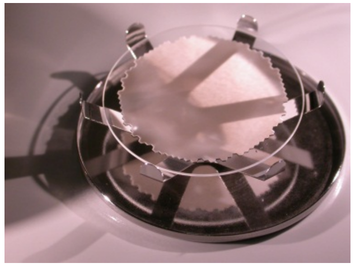

Capillary plate
(3 cm diameter)

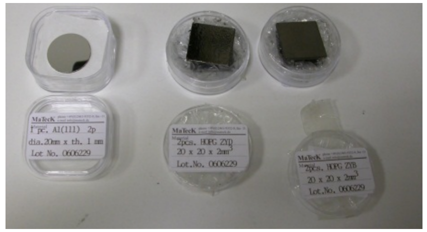

Aluminum and Graphite crystals.

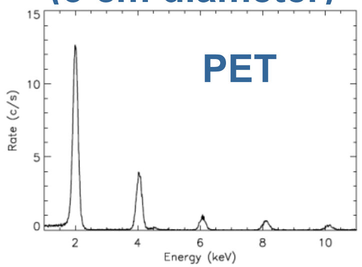

Spectrum of the orders of diffraction from the Ti X-ray tube and a PET crystal acquired with a Si-PiN detector by Amptek

(Muleri et al., SPIE, 2008)

Experimental set-up for the measurements of modulation factor and energy resolution.

Experimental set-up

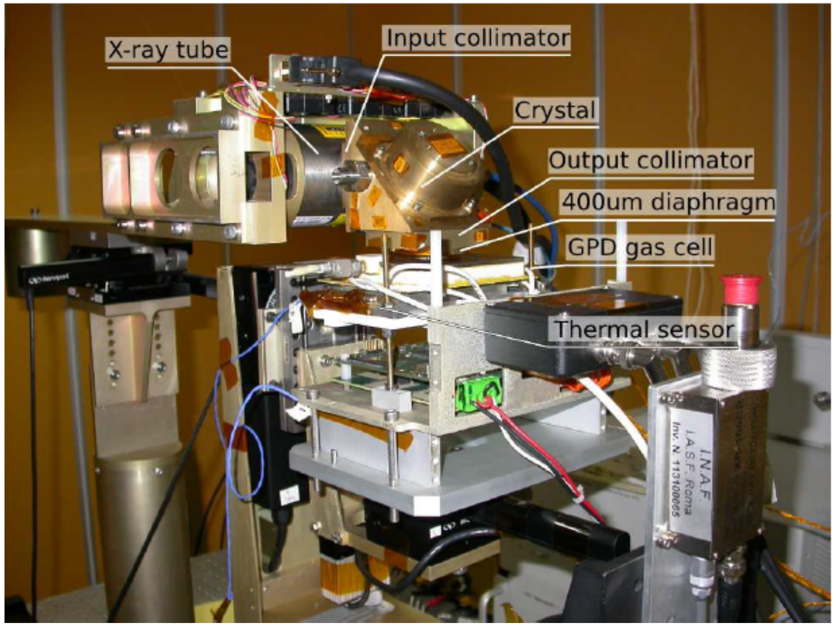

Hamamatsu 3.7 keV polarized source

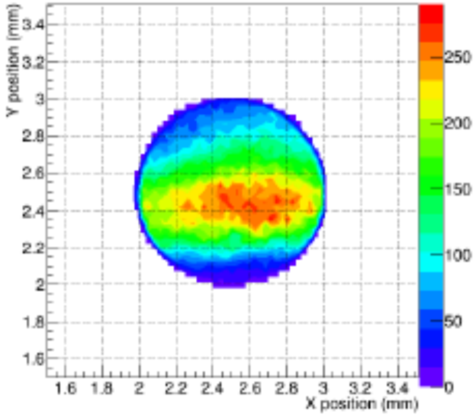

Impact Point map - 3.7 keV, 2772

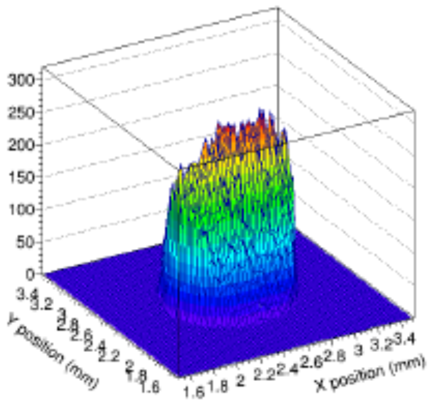

Oxford X-ray polarized source

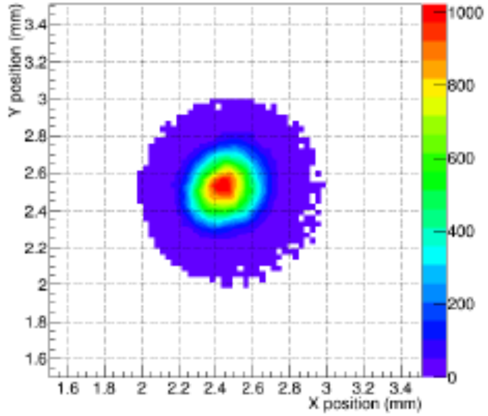

Impact Point map - 4.5 keV, 2736

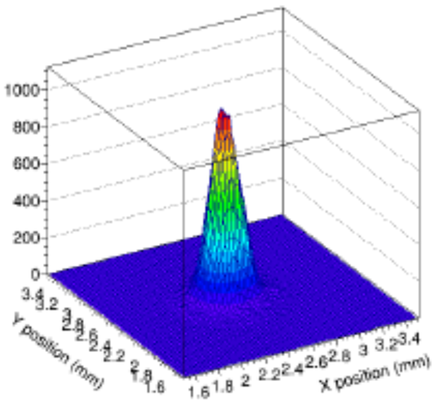

GPD Energy Resolution

Filling date:
4th November 2011

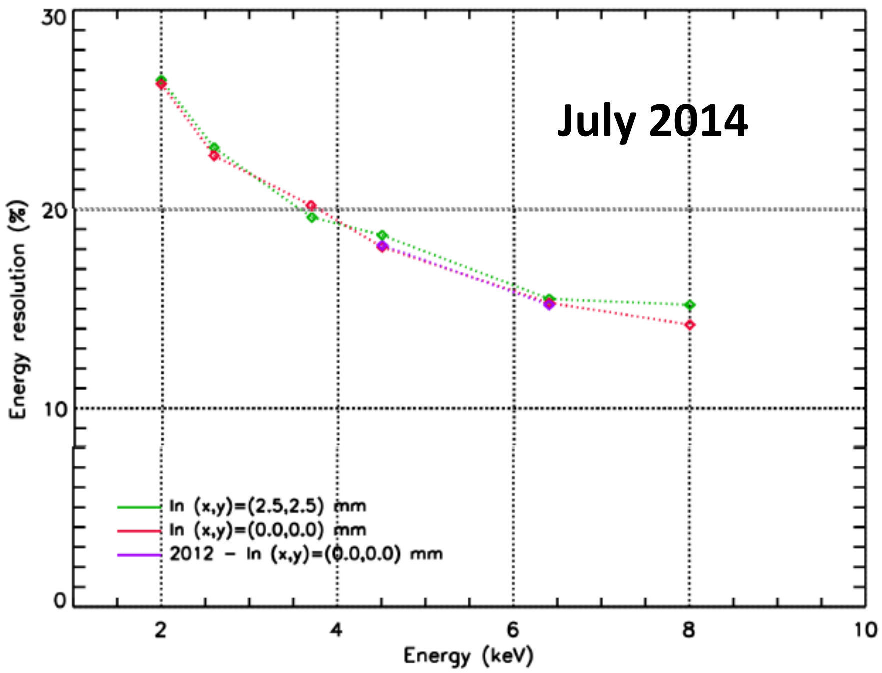

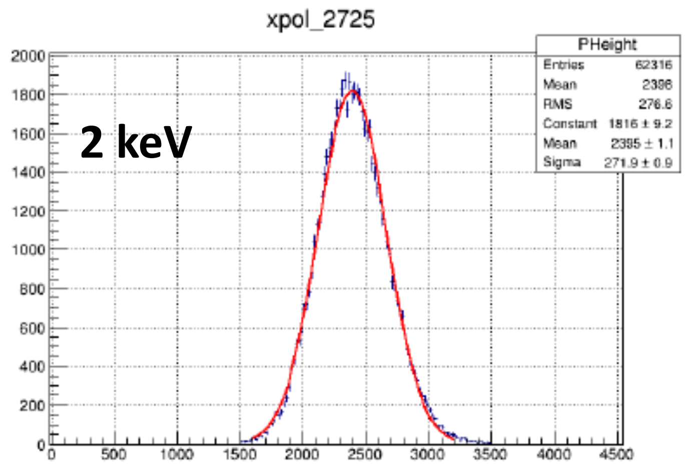

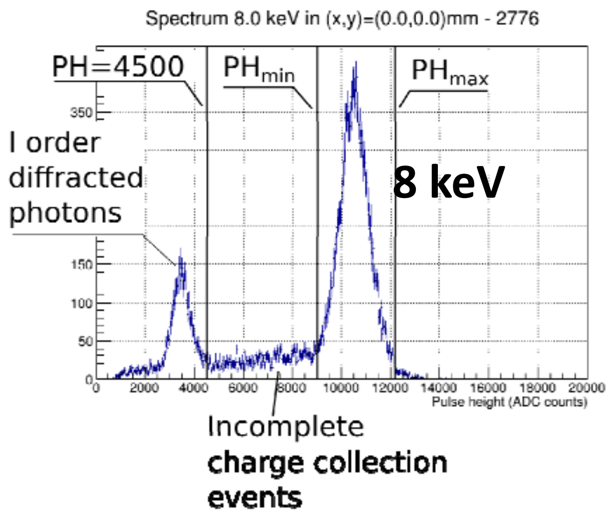

Modulation curves and their analysis

2 keV 1st step

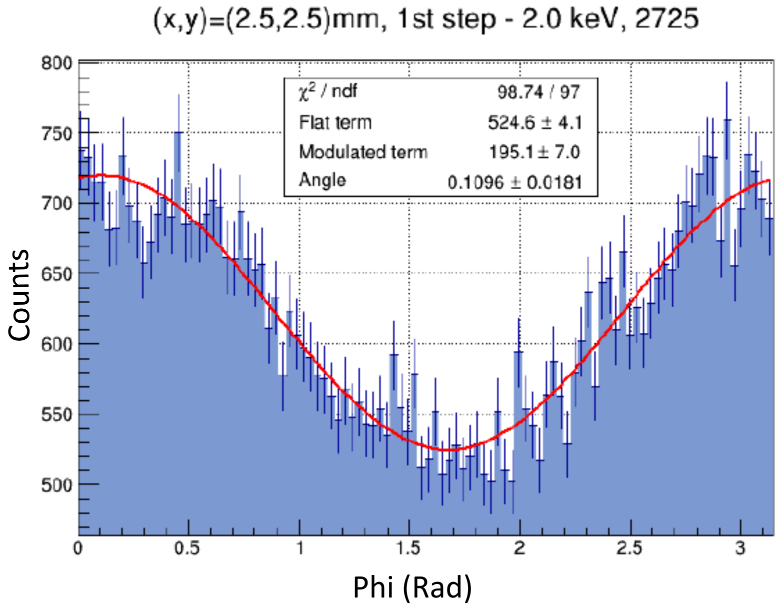

3.7 keV 2-step

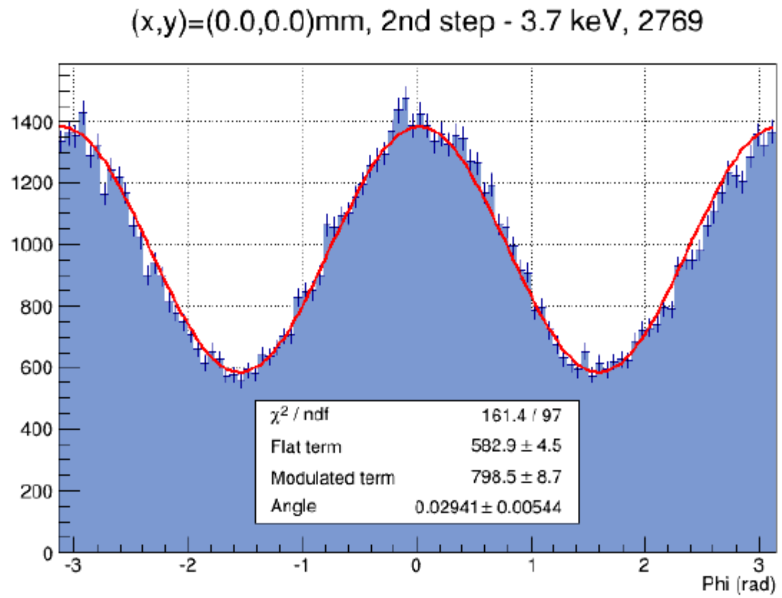

Modulation factor measurements and simulations

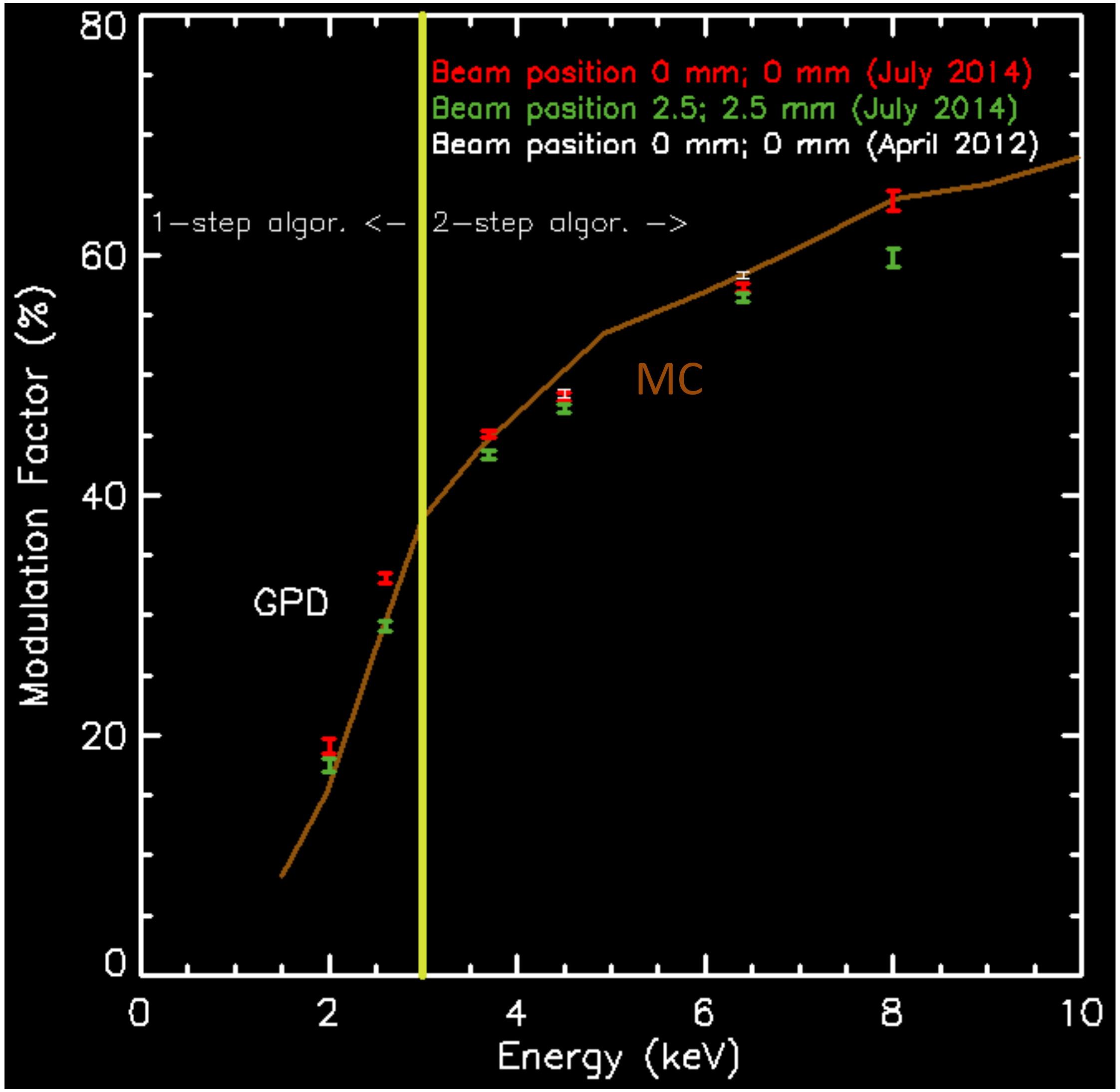

Measurement of the level of absence of residual modulation

- Check on the control of absence of systematics with Fe^{55} source at the moment (5.9 keV).

Many celestial source are expected to be highly polarized, however :

To measure 2 % of polarization (modulation of ~1%) the systematics should be understood/eliminated at level well below 1%.

Old design more than 10^6 counts

New Design 125 kcounts:
Modulation factor: ~50%
Residual modulation measured: ~0.54%
Residual polarization measured: ~1%
MDP 99% with μ=50% and 125 kc: ~ 2.3%

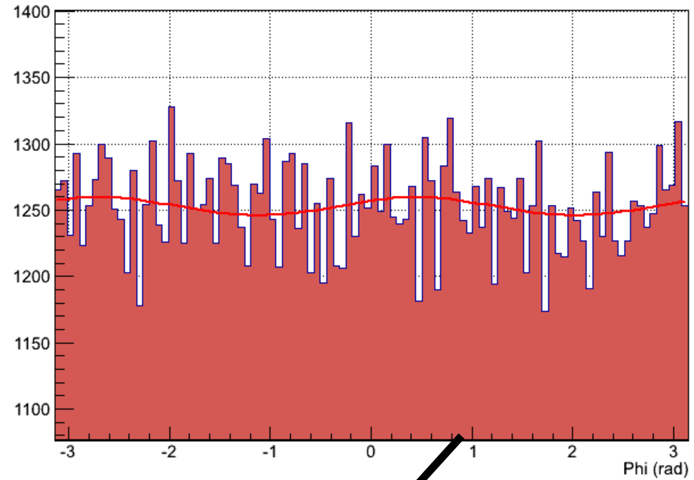

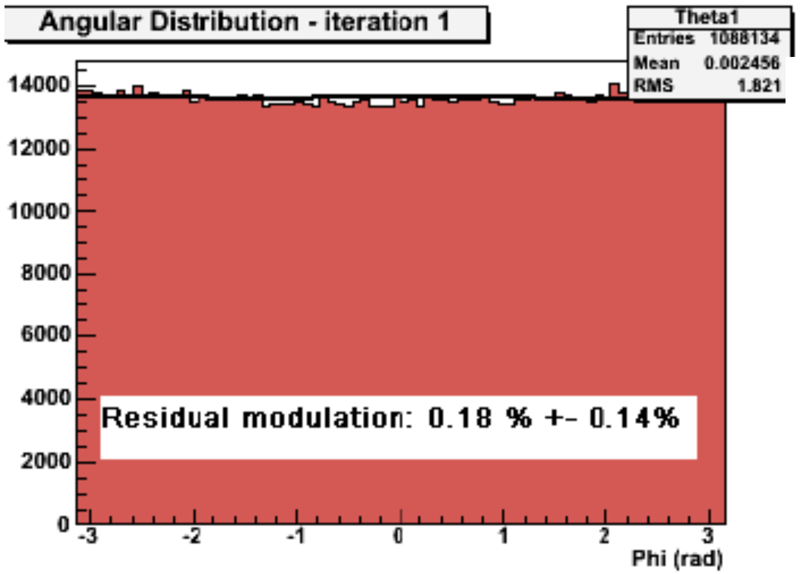

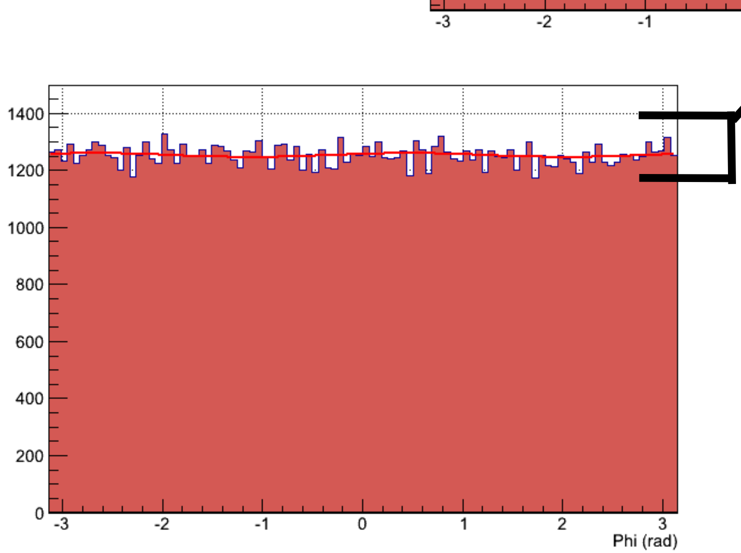

Imaging capabilities

1-step beam scan with a slit and Si-Pin

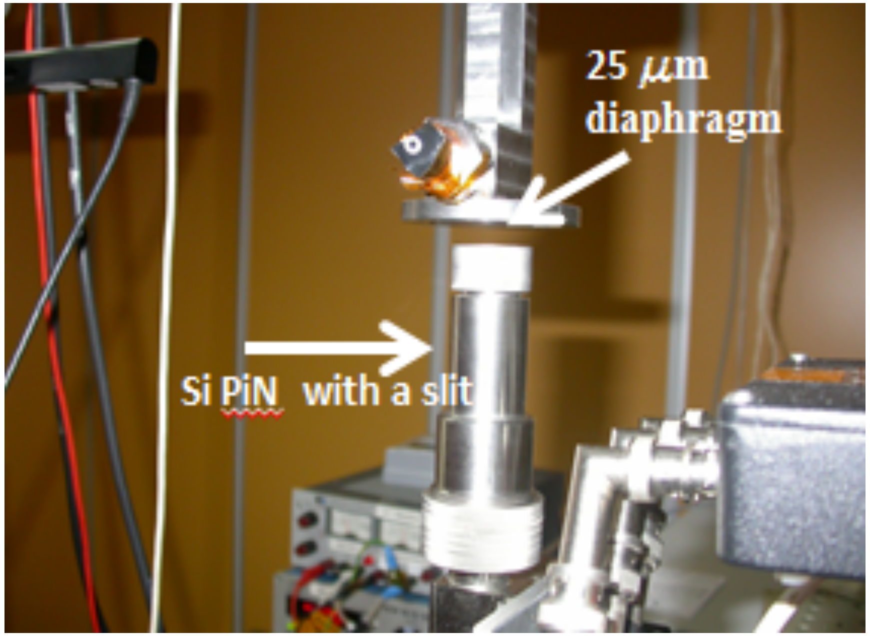

2-step acquisition with the GPD

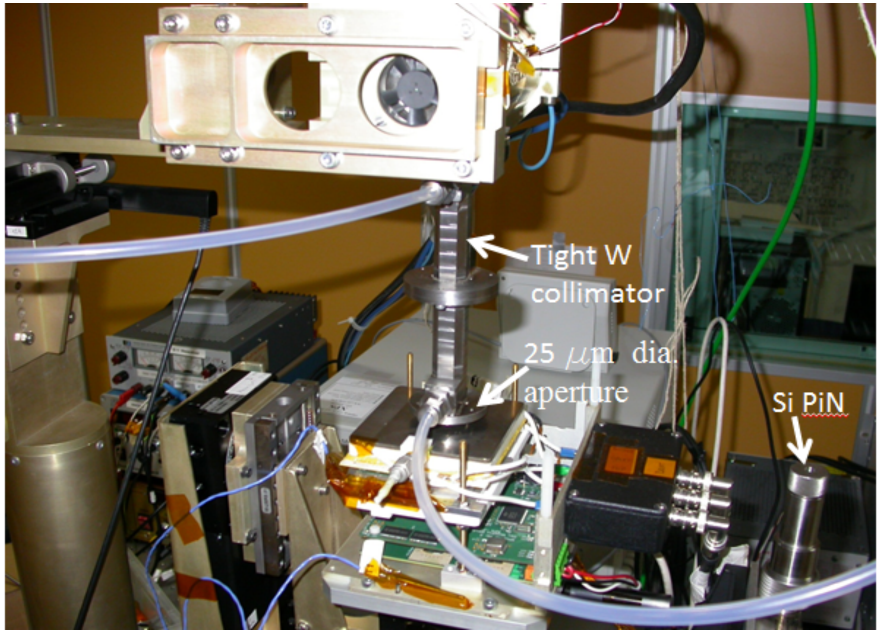

Beam scan with a slit and Si-PiN
2.3 keV (Mo X-ray tube)

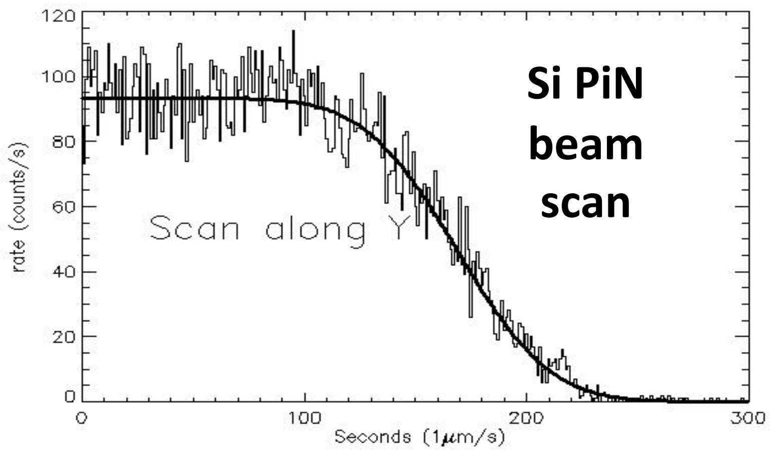

$$f(x) = \frac{A_X}{2}\left[1 - erf\left(\sqrt{2}\left(\frac{X - X_0}{2\sigma_X}\right)\right)\right]$$

σ_X	$\sigma(\sigma_X)$	χ
11.7 μm	0.5 μm	165.3/135
σ_Y	$\sigma(\sigma_Y)$	χ
32.9	0.9 μm	269.6/251

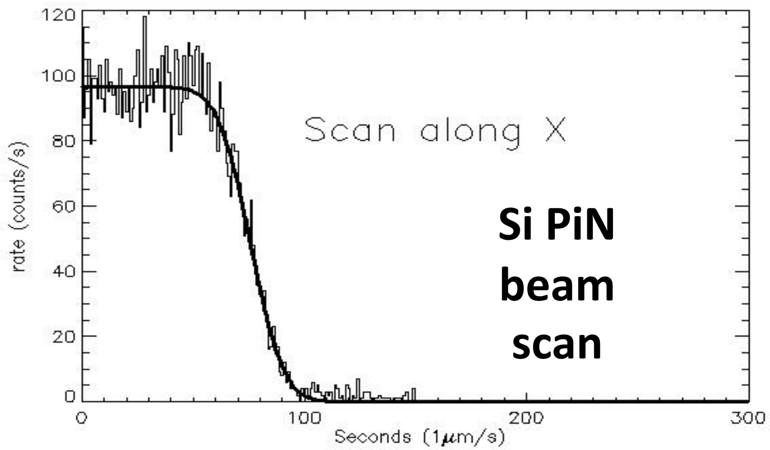

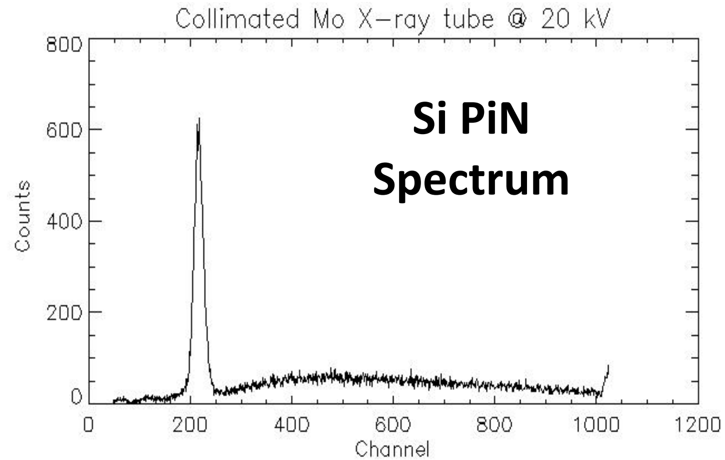

Images of collimated beams

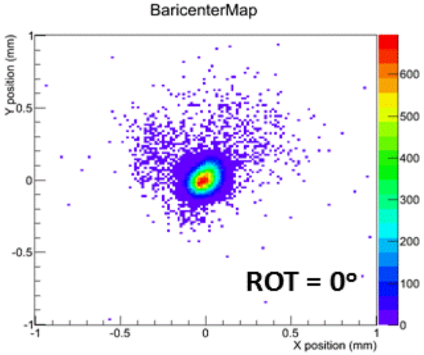

(0,0) mm

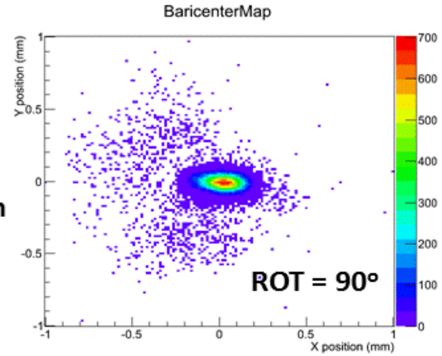

2.3 keV

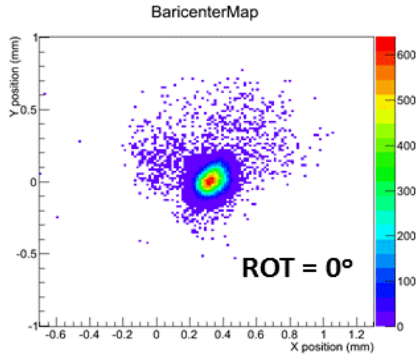

(0.3,0) mm

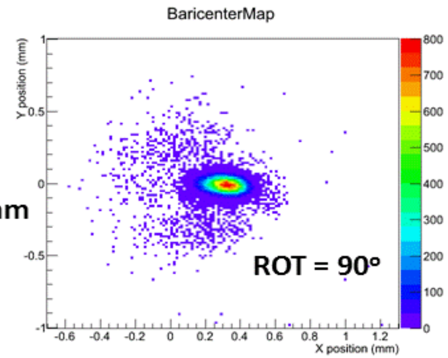

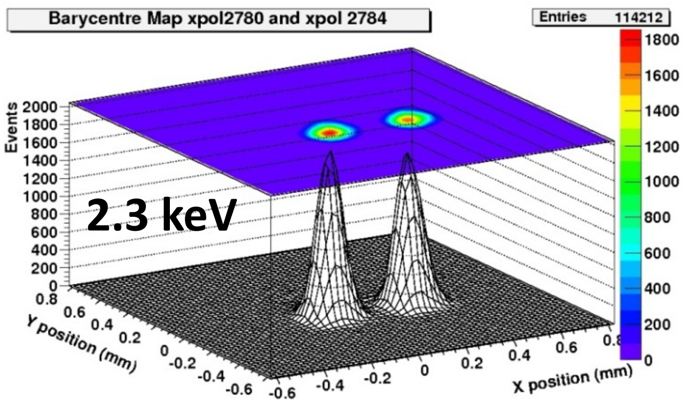

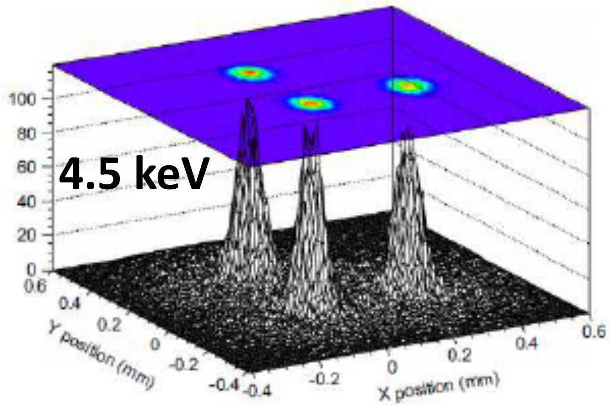

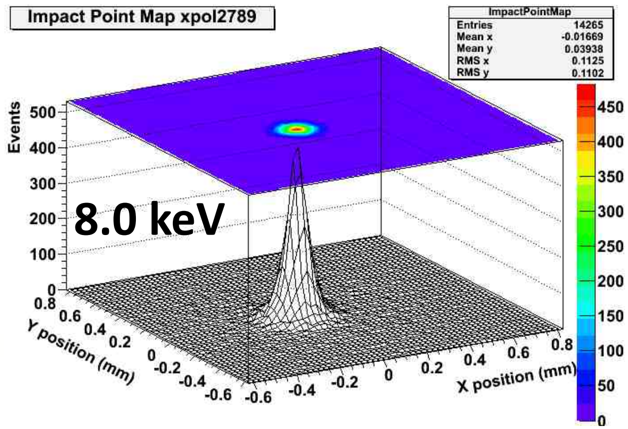

300 mm shift

XIPE proposed as ESA SM1 AOO

- 2 X-ray Telescopes From the JET-X Program
- GPD detectors already sudied for XEUS and IXO Program
- The standard bus of IRIDIUM Program

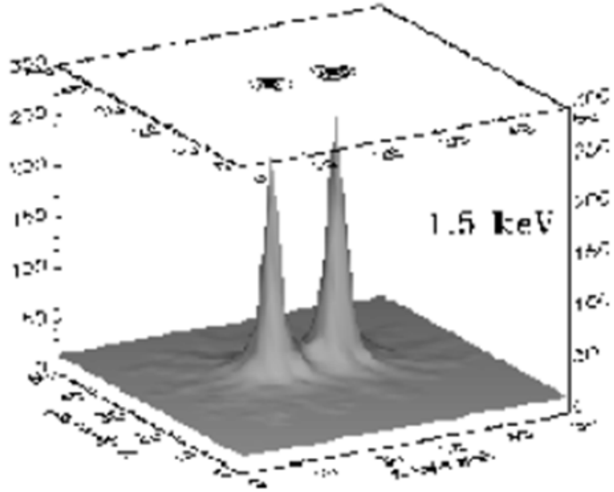

PANTER X-ray test facility.

At our knowledge this was the first time that an astronomical X-ray polarimeter was calibrated at the focus of an X-ray optics

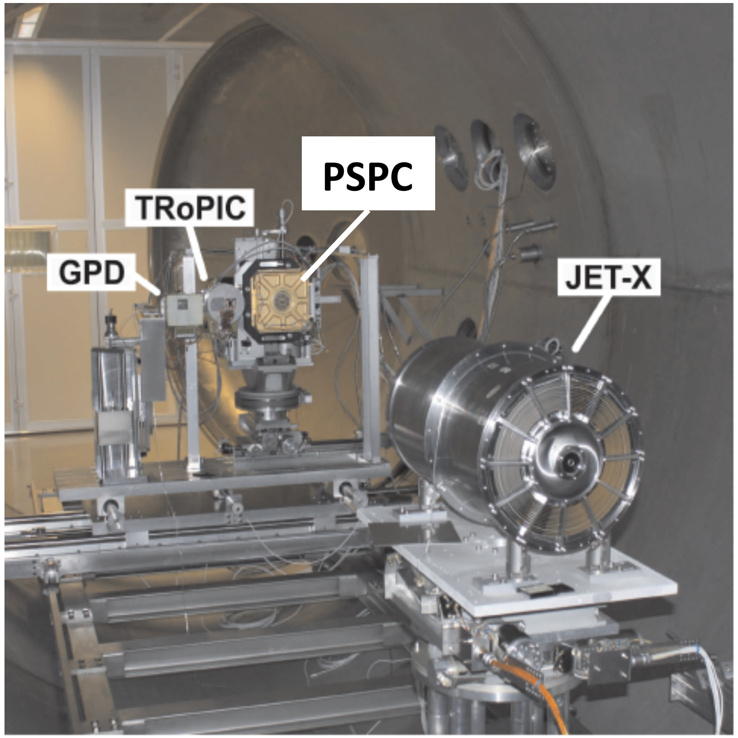

Figure 2. Measurement set-up in the vacuum chamber at PANTER.
(A color version of this figure is available in the online journal.)

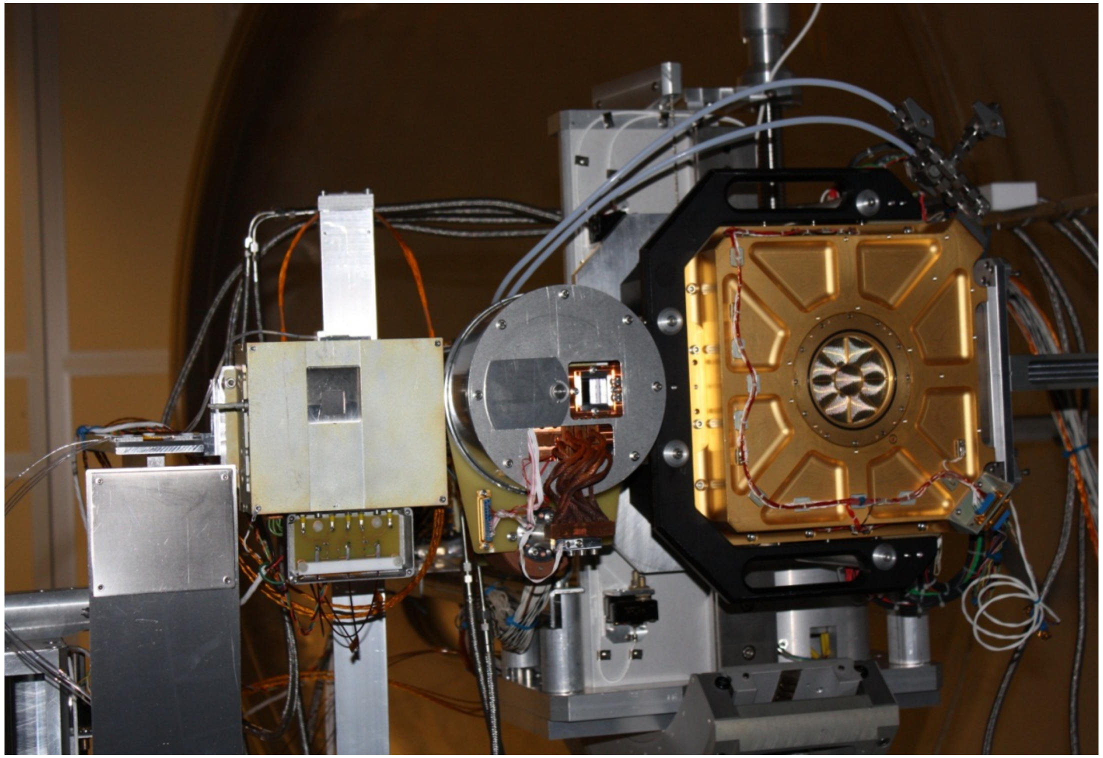

The imaging properties of the GPD.

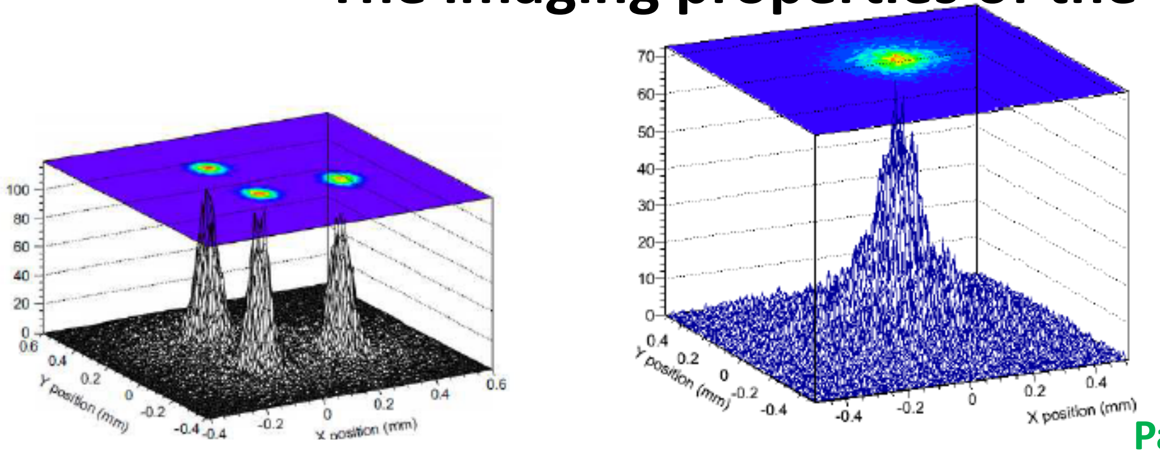

Spiga et al., 2013, Fabiani et al. 2014

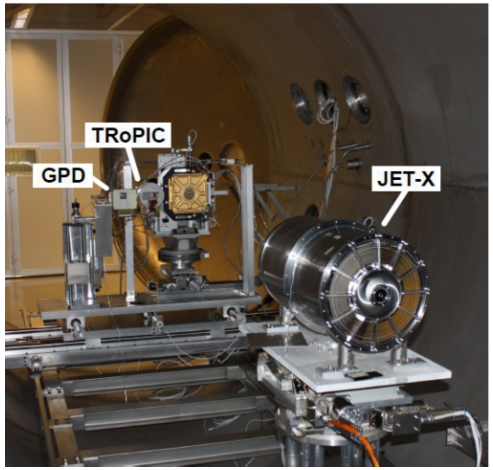

Panter X-ray facility (MPE, Germany):

JET-X (Telescope, same as Swift, ~1mm/arcmin)

Focal Length (3.5 m)

JET-X HEW (4.5 keV, 4.5 keV) : 18’’

JET-X + GPD (HEW) : 23.2’’ (394 μm)

IAPS/INAF laboratory :

Very narrow pencil beam.

Detector shifts : 300 μm.

Position resolution : 30 μm (rms).

Half Energy Width : 93 μm

Imaging properties driven by the optics.

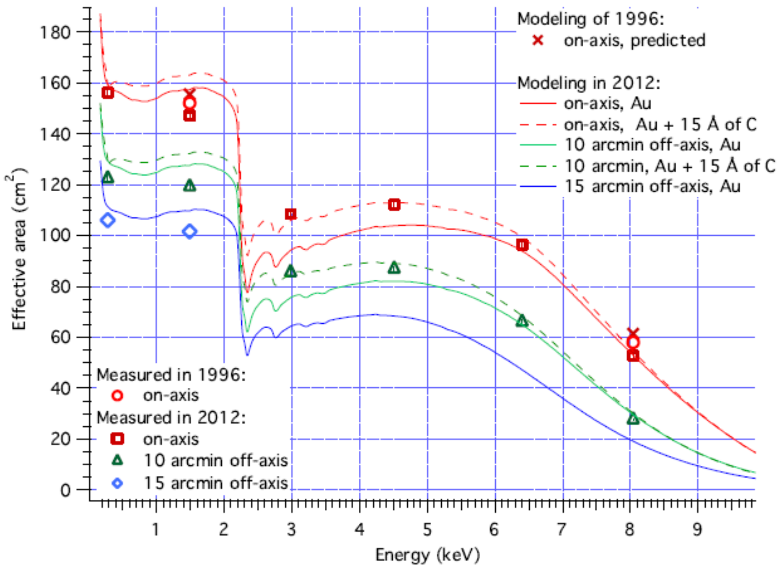

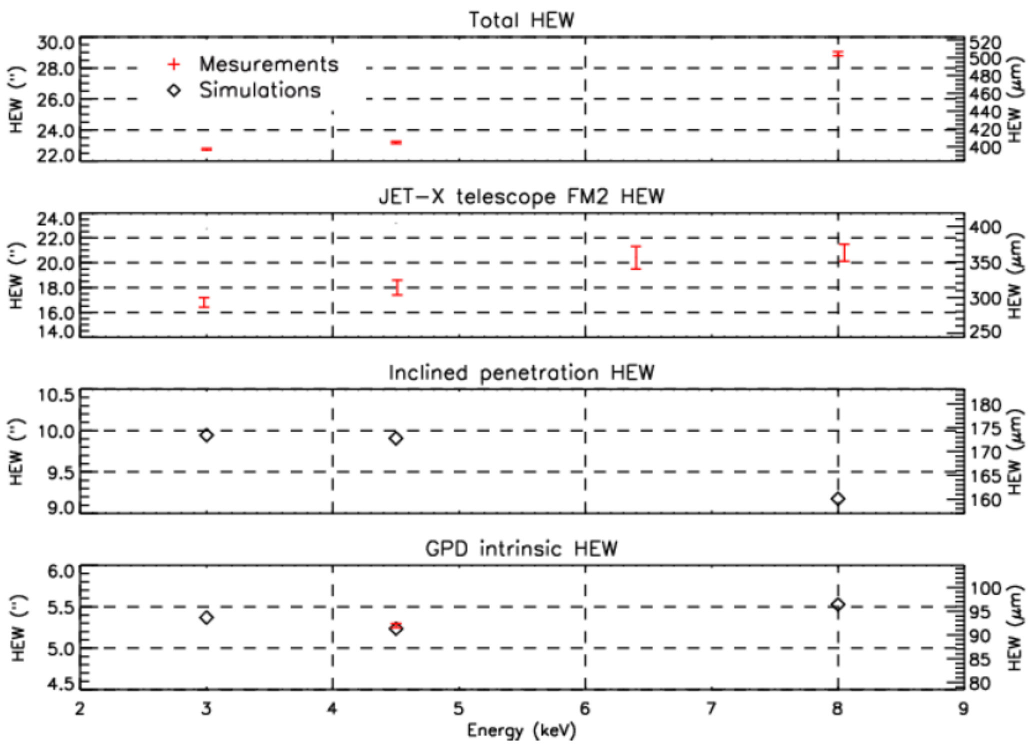

‘*In*’ and ‘*out*’ focus

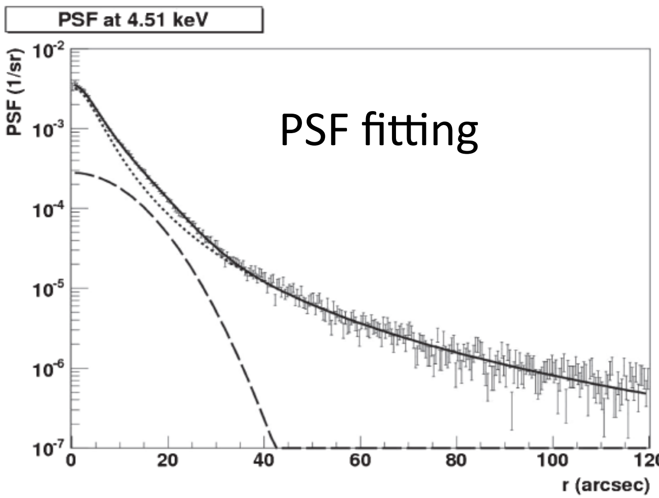

Figure 6. Fit performed on the PSF at 4.51 keV with a Gaussian plus a King function. The fit is performed on the radial coordinate θ from 0 to 120 arcsec. See Table 2 for the fit results at the energy of 2.98, 4.51, and 8.05 keV. Each fit is performed on the radial coordinate θ from 0 to 120 arcsec and the IPs density distribution is normalized to the total number of counts.

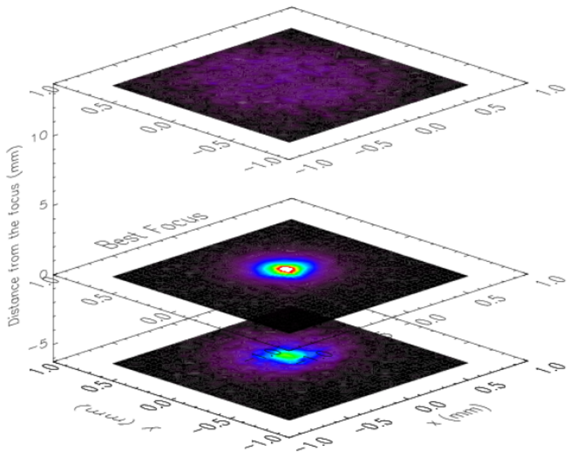

Figure 4. IP maps obtained for three different distances between the GPD and the telescope optics. The plots are normalized to the number of counts for each image. At the central position the image corresponding to the better angular resolution is shown. A narrower PSF core (white spot) with respect to the other images is present in this one.

(A color version of this figure is available in the online journal.)

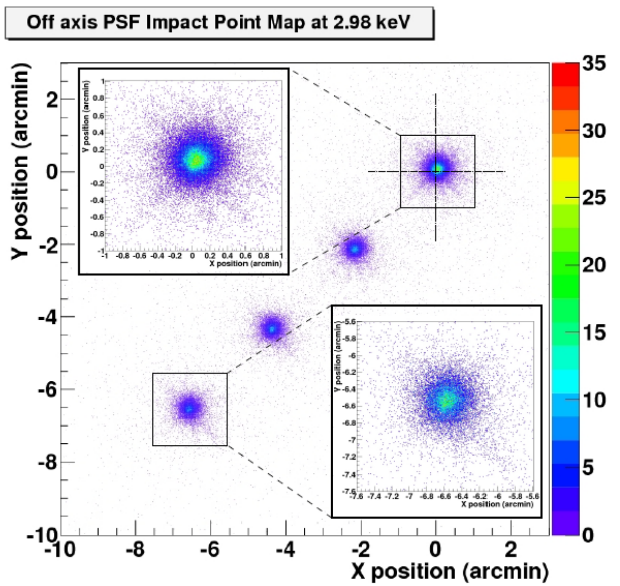

Fabiani et al., 2014

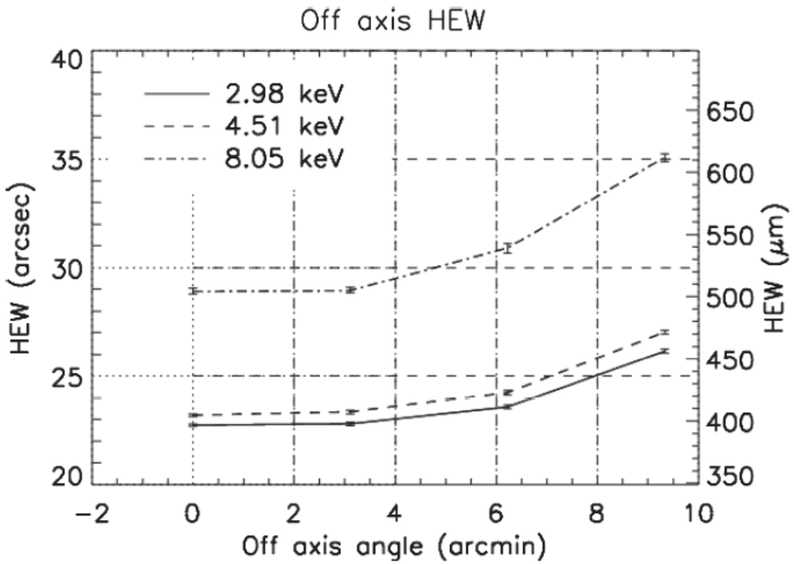

Figure 10. Off-axis HEW at 2.98, 4.51, and 8.05 keV. Plotted values are listed in Table 3. The FOV of JET-X coupled with the GPD (see Table 1) corresponds to an angle of 10.4 arcmin from the image center to the corner along the diagonal.

GPD imaging performances @ PANTER

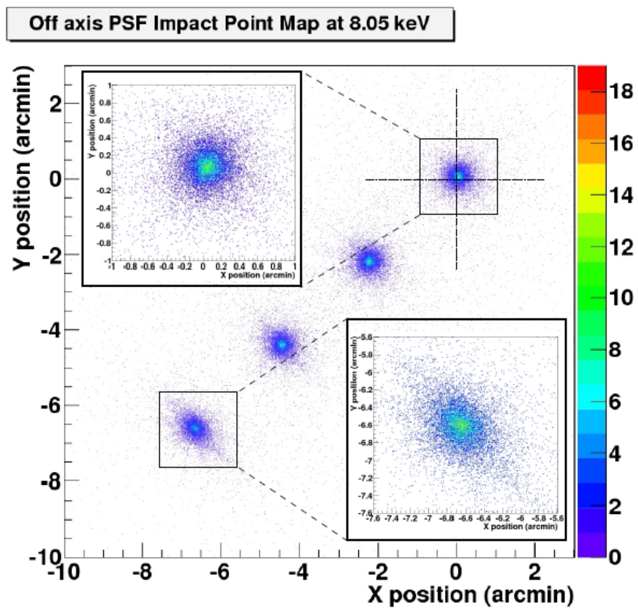

Imaging allows for measuring gas parameters

Imaging allow for making a diagnostic and measuring the attachment coefficient a (cm^{-1}).

Inclining the detector with respect to a narrow X-ray beam is possible to put in correspondence the drift distance from the impact point with the X&Y coordinates in the readout plane

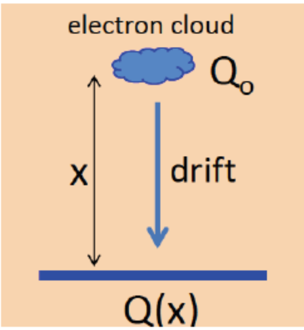

$$Q(x) = Q_0 e^{-\alpha x}$$

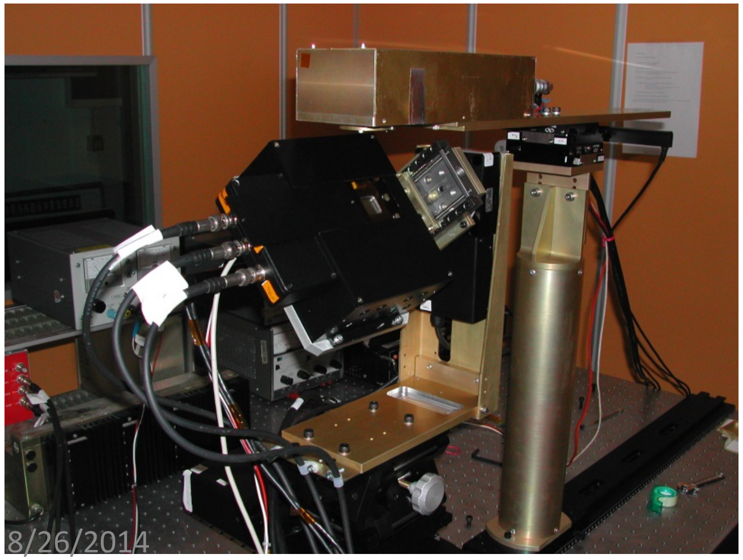

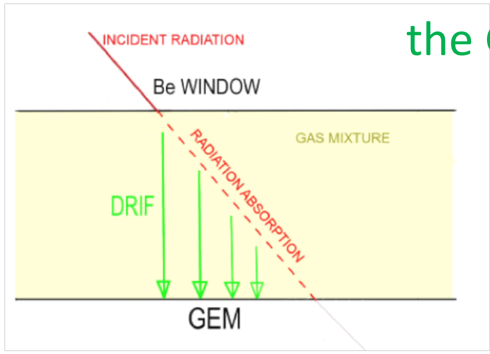

Events close to the GEM

Events close to the window

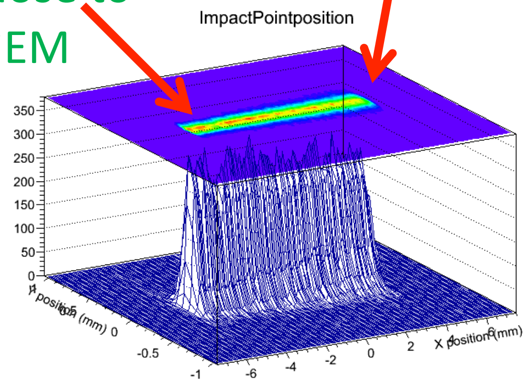

The image of a narrow pencil beam is a '*strip*' on the GPD readout plane :

$$z_h = \tan(\theta) * (L-x)$$

z_h is the interaction height, θ is the inclination, L is the strip length, x is the position along the '*strip*'

The larger is the attachment coefficient the more rapidly decreases the pulse height with the drift distance. We measure this coefficient by fitting such decrement with respect to the reconstructed drift distance.

$$Q(x) = Q_0 e^{-\alpha x}$$

Hill et al., 2013

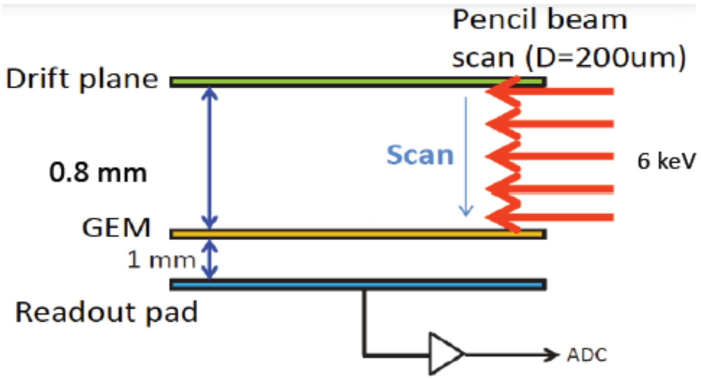

electrons attach to contaminants and do not reach the detection strips, thus
t allows the measurement of the electron capture coefficient, α.

In GEMS/TPC the drift is scanned with a pencil beam to measure a(cm^{-1}).

We make one pencil beam and we incline the detector using imaging.

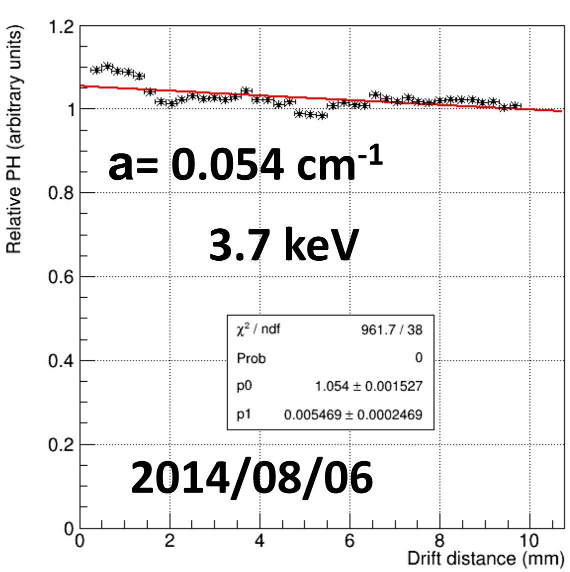

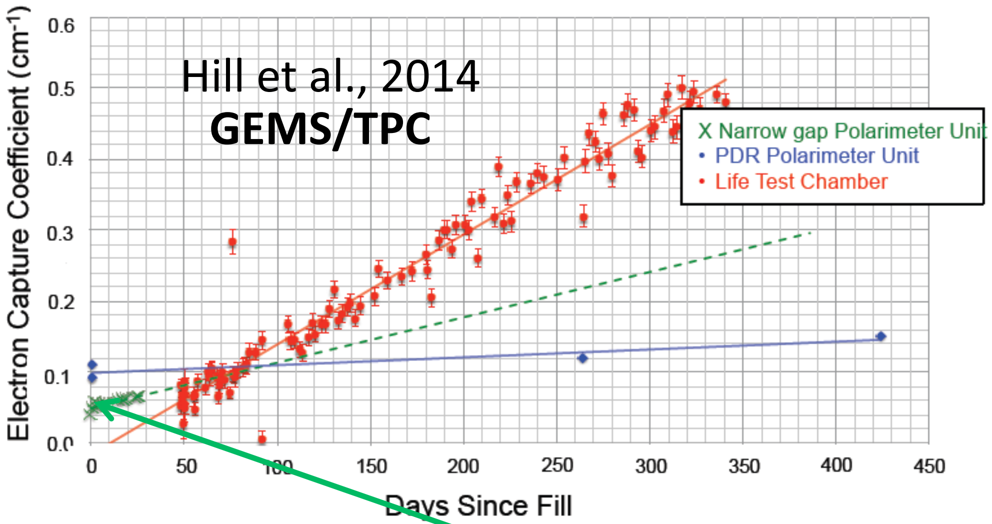

GPD is here but 819 days since fill !

GPD filled 2011/11/4

Energy resolution stability
GPD

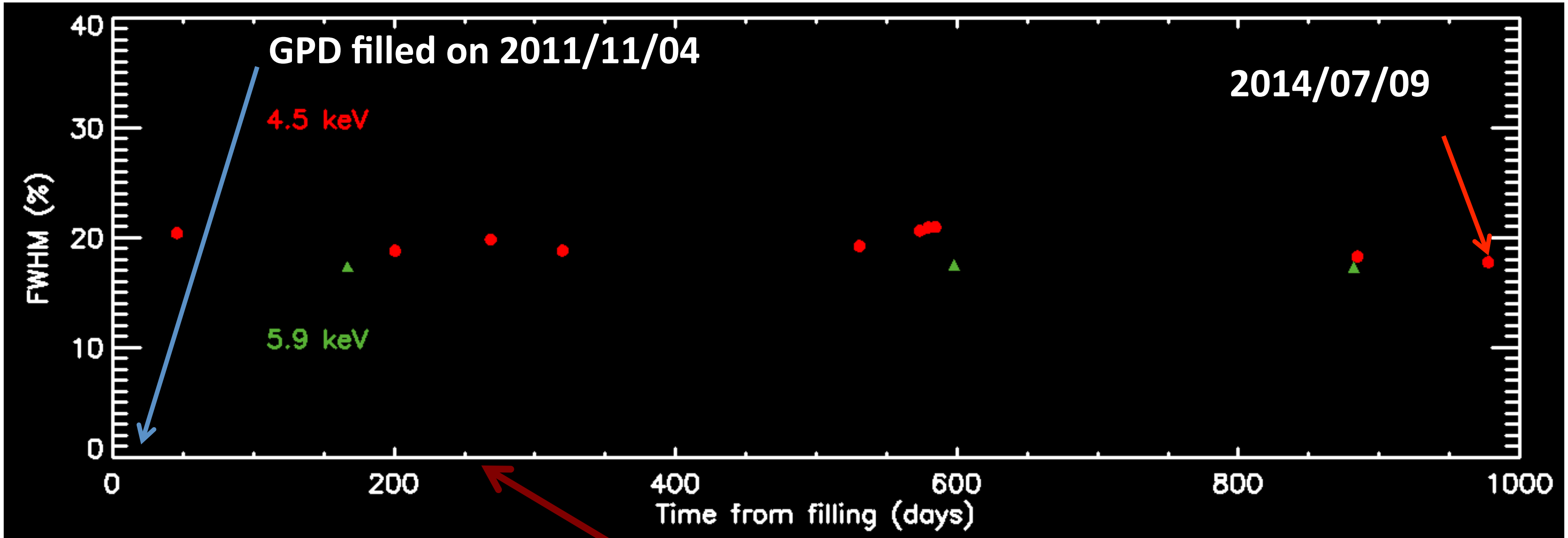

Measured GPD energy resolution (FWHM, %)

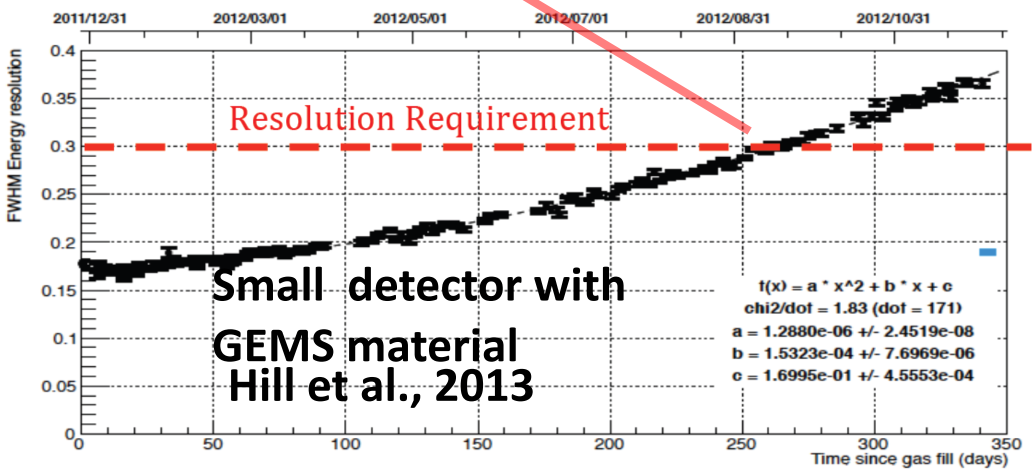

compared to what has been measured@GODDARD on a small detector using the same GEMS material.

Hill J. et al. rescaling to flight model volume estimates 23 years in orbit

We are not rescaling : this is the real detector.

Comparison of the Sensitivity of GPD vs TPC

Is so large the difference in sensitivity of the GPD with respect to a TPC ?

TPC : L = 32 cm; P = ¼ Atm **GPD : L = 1 cm; P = 1 Atm**

A factor of 8 in efficiency that means a factor of 2.8 in sensitivity. Is it really like that ? :

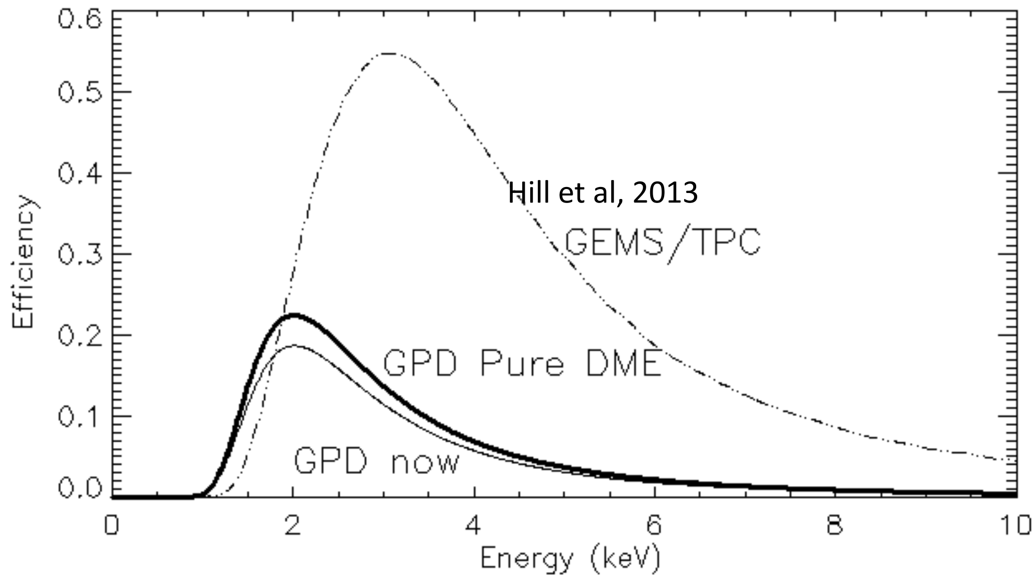

The peak efficiencies ratios is only 2.7

Dead layer

Window

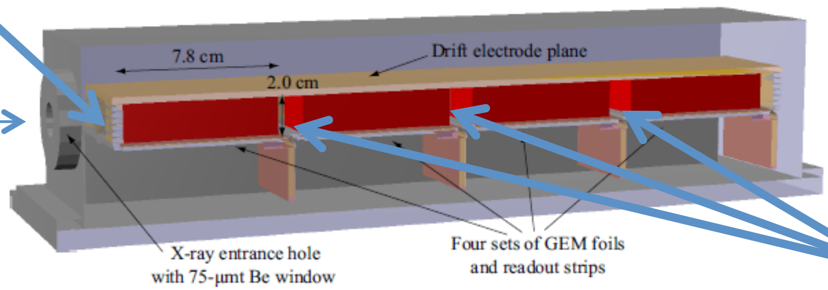

GEMS/TPC

Kitaguchi et al., 2014

Dead Layers

Modulation Factor

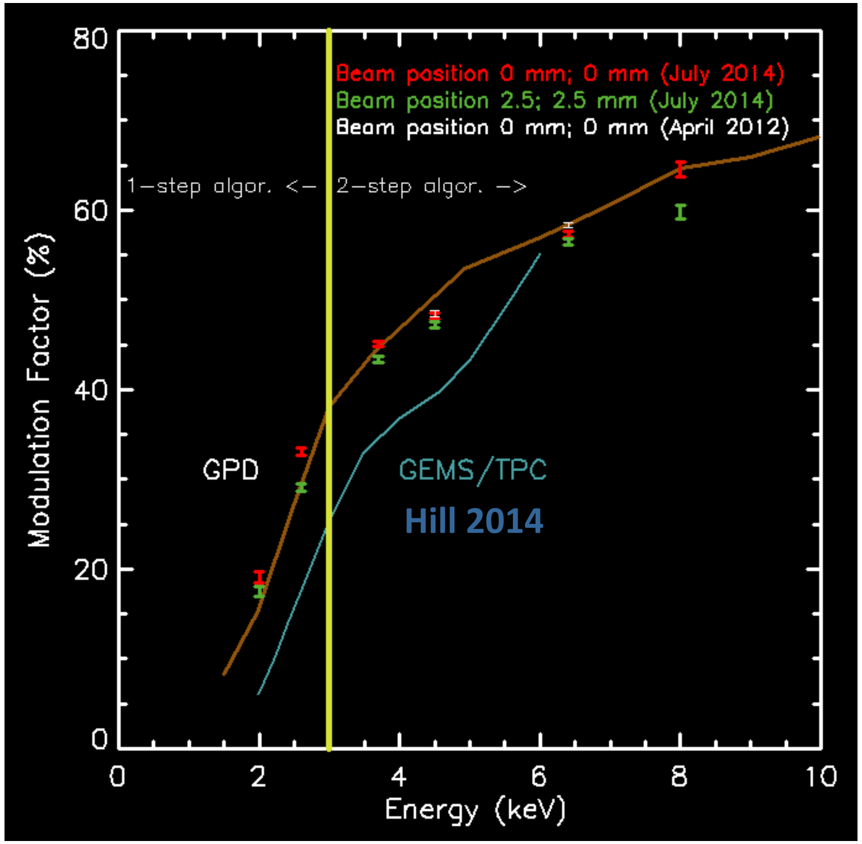

The modulation factor of the GPD is larger with respect to the TPC in the energy range of best sensitivity.

- Smaller average drift distance.
- Freedom in choosing the drift field by selecting the minimum transverse diffusion.

What if we place the GPD at the focus of the GEMS mirror ?

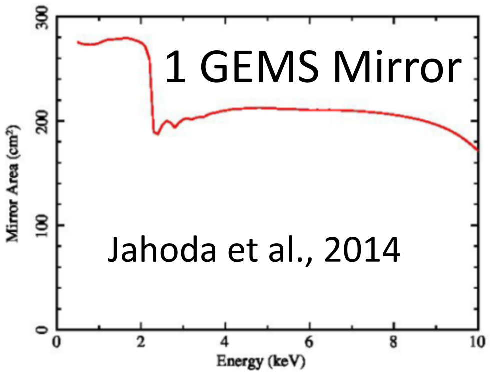

$$MDP(99\%) = \frac{4.29}{\mu R_S}\sqrt{\frac{R_S + R_B}{T}}$$

R_S Source rate
R_B Backg. rate
μ Modul. Factor

Bright source:
MDP GPD = 1.7 MDP GEMS

Faint source:
Background ?

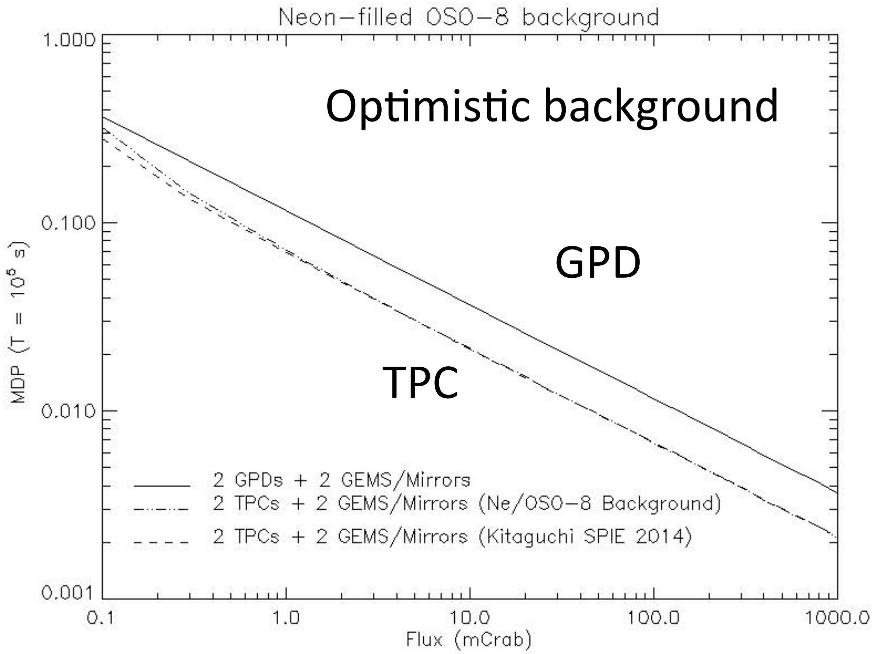

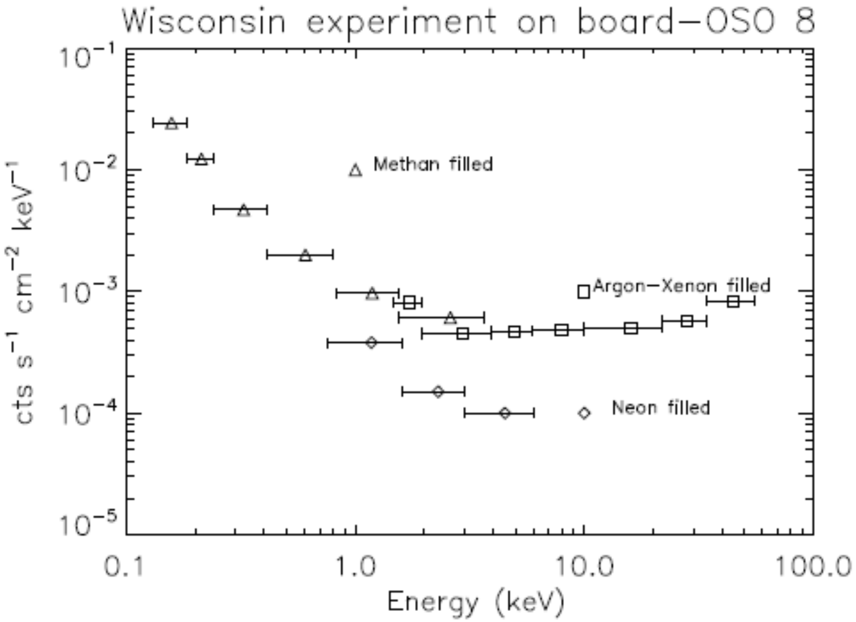

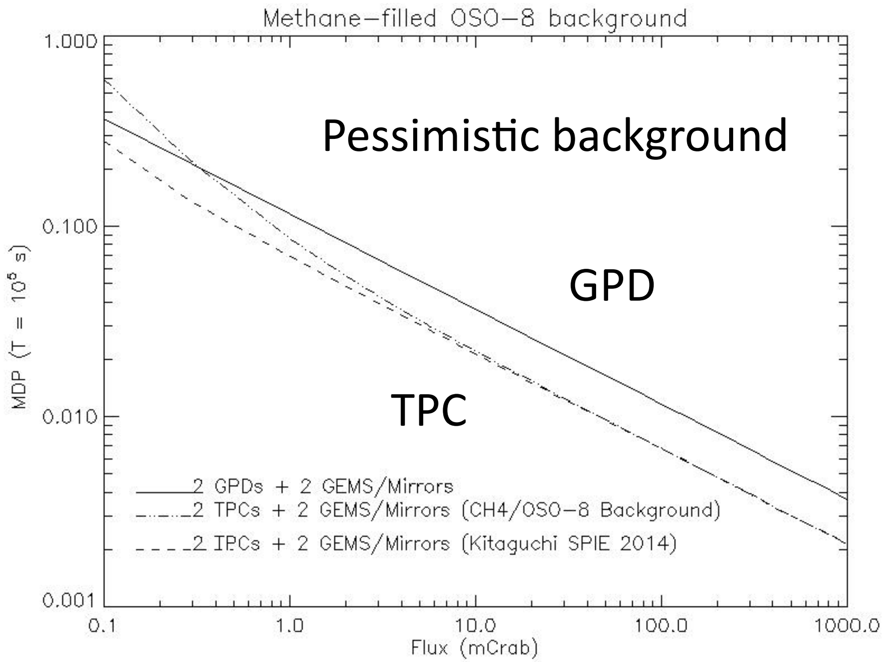

A Medium Energy X-ray polarimeter

The GPD can work between 2 – 35 keV choosing a proper mixture/pressure

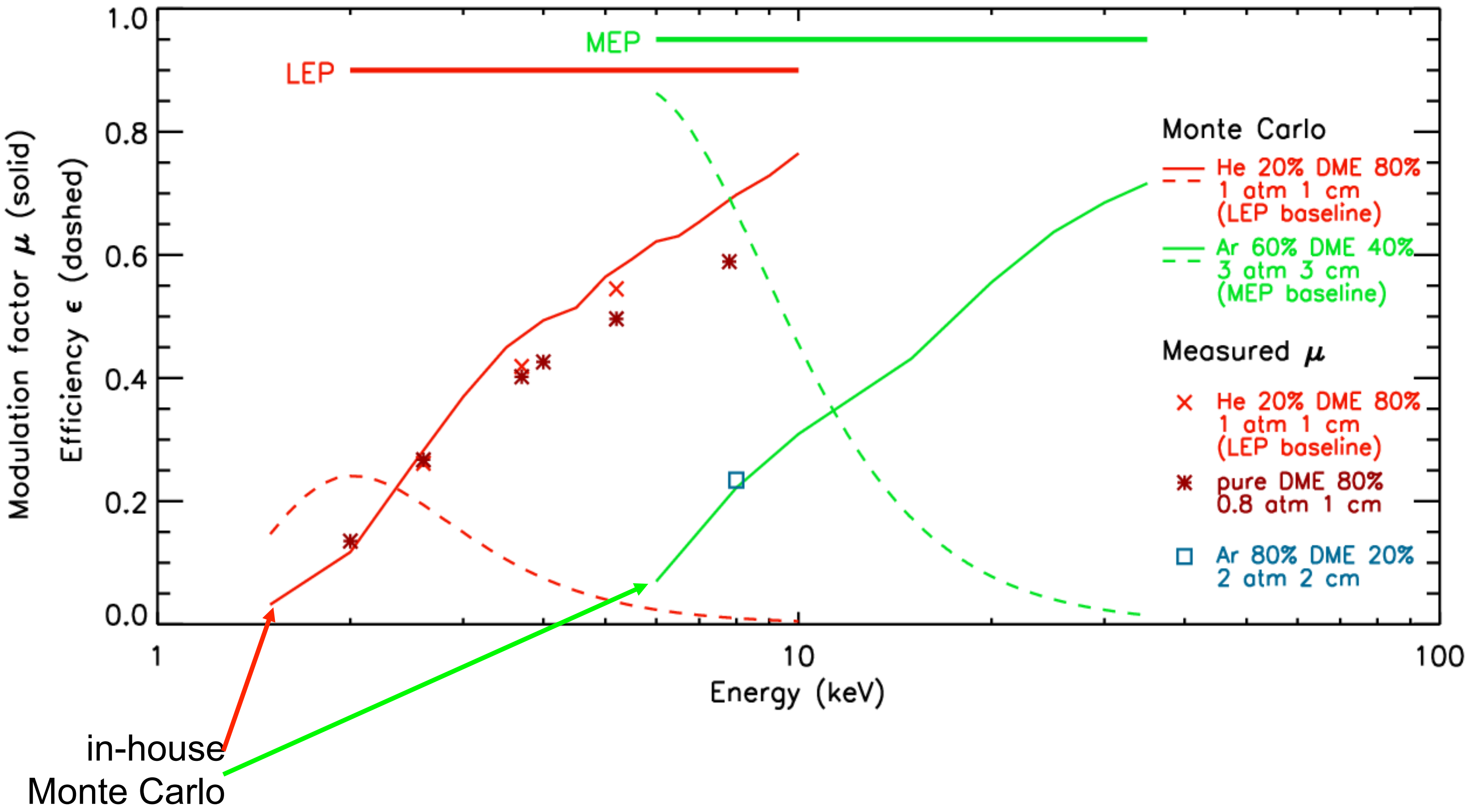

MEP - State of the art

Current prototype

Argon 70% DME 30% 2 cm, 2 bar

Goal

- Argon mixture @ 3 bar
- Gas cell thickness 3cm
- new ASIC (already being manufactured)
    - Reduce the ROI
    - Increase the clock

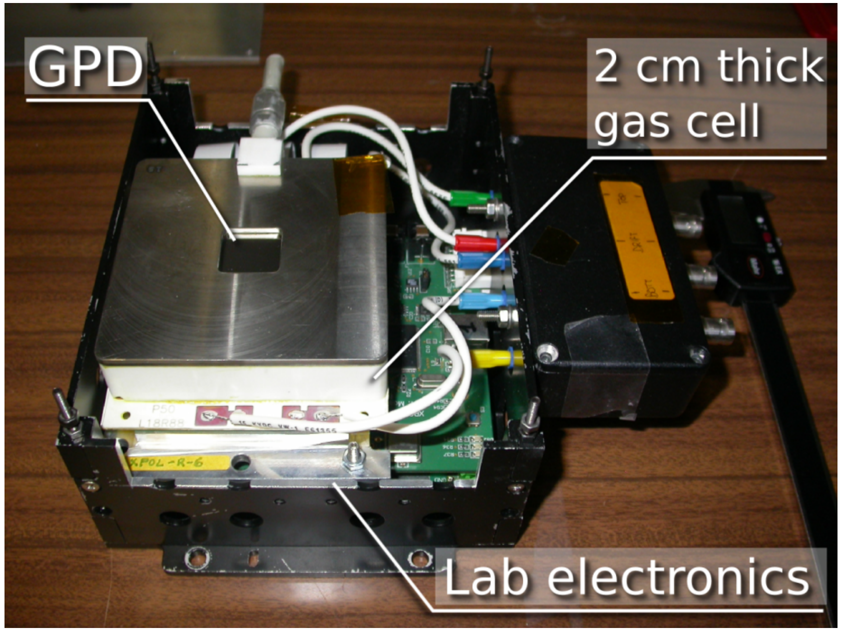

Real tracks @ 22 keV

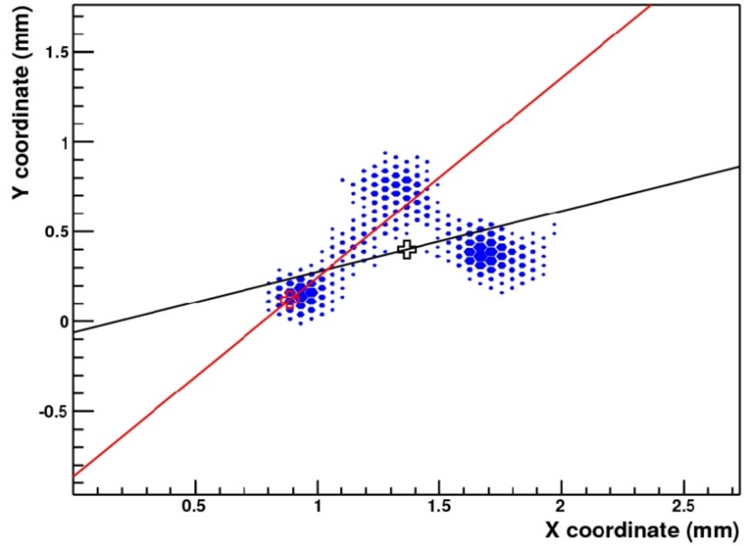

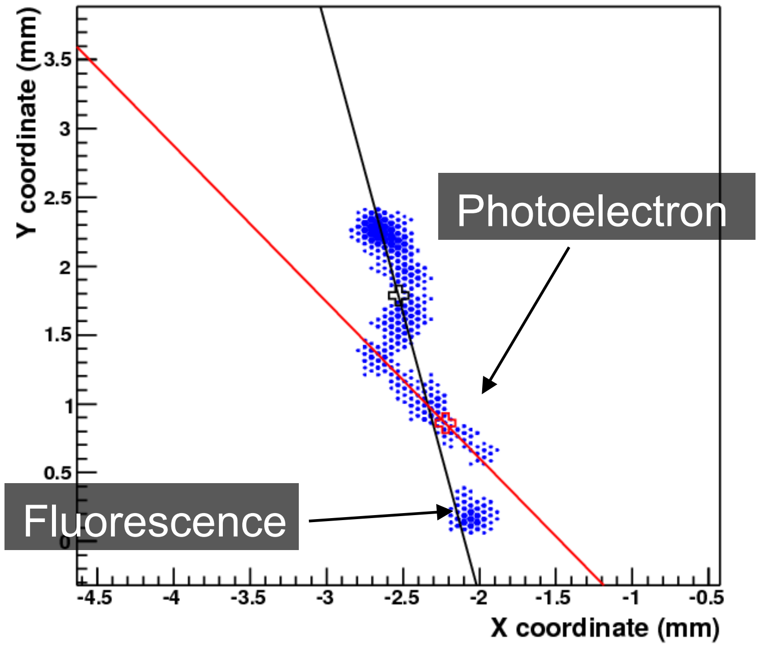

Why X-ray Polarimetry ?

Acceleration phenomena:

- Solar Flares
- Pulsar wind nebulae
- Shell-like Supernovae
- µQSO
- Blazar and radiogalaxy

Medium Energy X-ray Polarimeter

Imaging

Emission in strong magnetic fields:

- Emission in strong magnetic fields: magnetic cataclysmic variables
- Emission in strong magnetic fields: accreting millisecond pulsars
- Emission in very strong magnetic fields: accreting X-ray pulsars
- Emission in ultra strong magnetic fields : magnetars.

Scattering in aspherical situations :

- X-ray binaries
- Radio-quiet AGN
- X-ray reflection nebulae

Fundamental Physics :

Matter in Extreme Magnetic Fields: QED effects

Matter in Extreme Gravitational Fields: GR effects

Quantum Gravity

Search for axion-like particles

Solar flares

See talk of Valentina Zharkova on Thurday

Solar flares are believed to be triggered by magnetic reconnection at the top of magnetic loops in the corona with an acceleration of charged particles down to the chromosphere.

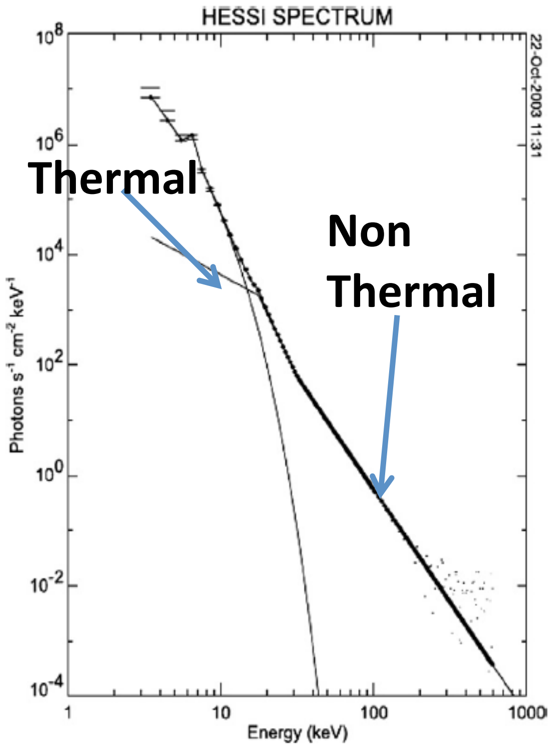

Fig. 6. The RHESSI X-ray spectrum of the hard X-ray source observed during the August 30, 2002 flare of class X 1.5 at 13:27:56-13:28:12 UT ($\Delta t = 16$ s). The spectrum is the sum of the thermal and non-thermal components (Karlický et al., 2004).

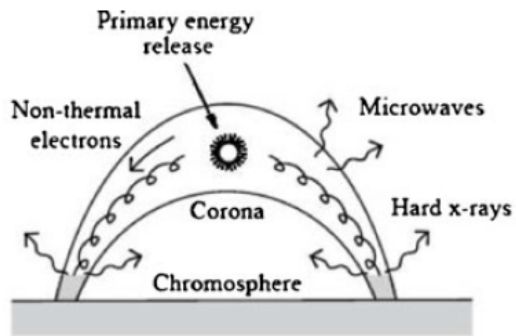

Hard X-rays : non thermal emission emitted mostly in footprints and in the coronal primary source.

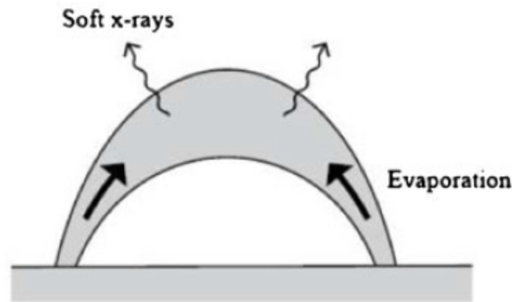

In soft **X-rays** (< 10 keV) the emission is mostly thermal.

The X-ray flux above 10-15 keV is expected to be polarized. P up to 40 % for a flare on the solar limb.

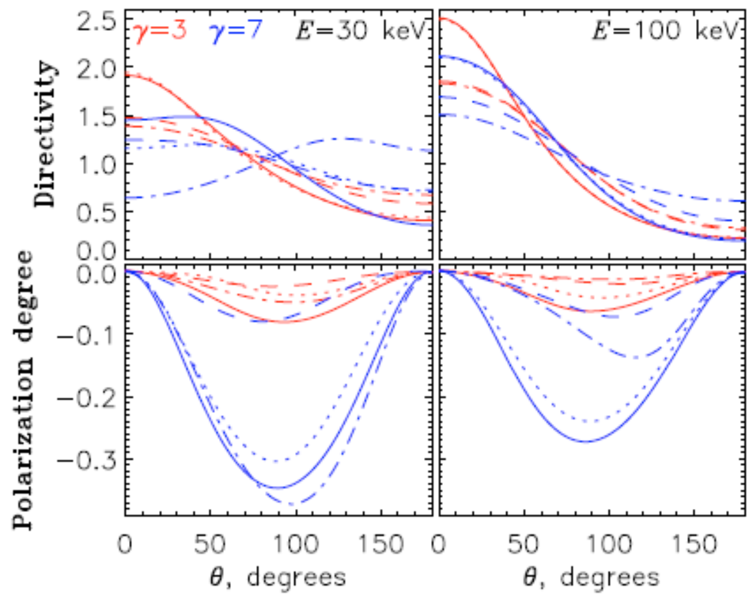

q angle between the radiation direction (**k**) and the normal (**p$_o$**) to the Sun on the onset-point.

P < 0 => **E** //(**p$_o$**^**k**)

Zharkova et al., 2010

Flare Class	Maximum X-Ray Flux watts per square meter (W/m^2)	Maximum X-Ray Flux ergs per square centimeter per second ($erg/cm^2 \cdot s$)
A*n*	$n \times 10^{-8}$	$n \times 10^{-5}$
B*n*	$n \times 10^{-7}$	$n \times 10^{-4}$
C*n*	$n \times 10^{-6}$	$n \times 10^{-3}$
M*n*	$n \times 10^{-5}$	$n \times 10^{-2}$
X*n*	$n \times 10^{-4}$	$n \times 10^{-1}$

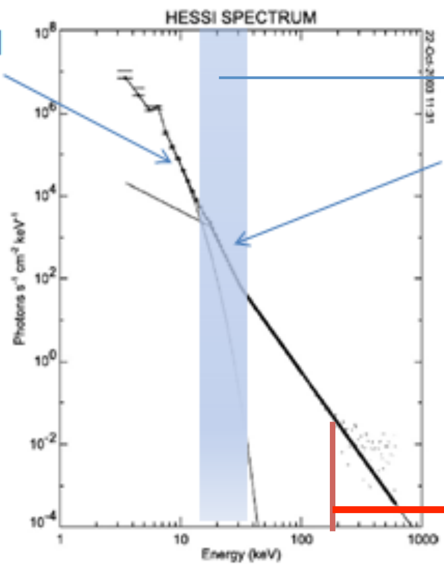

The energy band of the GPD covers a region where the flux is high and the non thermal emission stars to overcome the thermal emission.

Geometrical area is small such as the background is small

Solar Energetic Emission and Particles Explorer (SEEPE)

Siming Liu
Purple Mountain Observatory
Paolo Soffitta, IAPS/INAF
Ronaldo Bellazzini, INFN-Pisa
Robert Wimmer-Schweingruber, CAU Kiel

Will provide light-curves, spectra, polarization of hard X-rays and information on the transport of charge particles in solar flares

Scientific Payload

Institute for Space Astrophysics and Planetology
Istituto di Astrofisica e Planetologia Spaziali

A solar flares X-ray polarimeter

S. Fabiani[1,3], R. Bellazzini[2], F. Berrilli[3], A. Brez[2], E. Costa[1], F. Muleri[1], M. Pinchera[2], A. Rubini[1], P. Soffitta[1], and G. Spandre[2]

$$\mathrm{MDP} = \frac{4.29}{\mu \cdot R} \cdot \sqrt{\frac{R+B}{T}}$$

Flare Class	MDP (%)	Integration Time (s)
X10	0.6	748
X5.1	1.3	989
X1.2	4.8	239
M5.2	6.6	489
M1	46.4	128

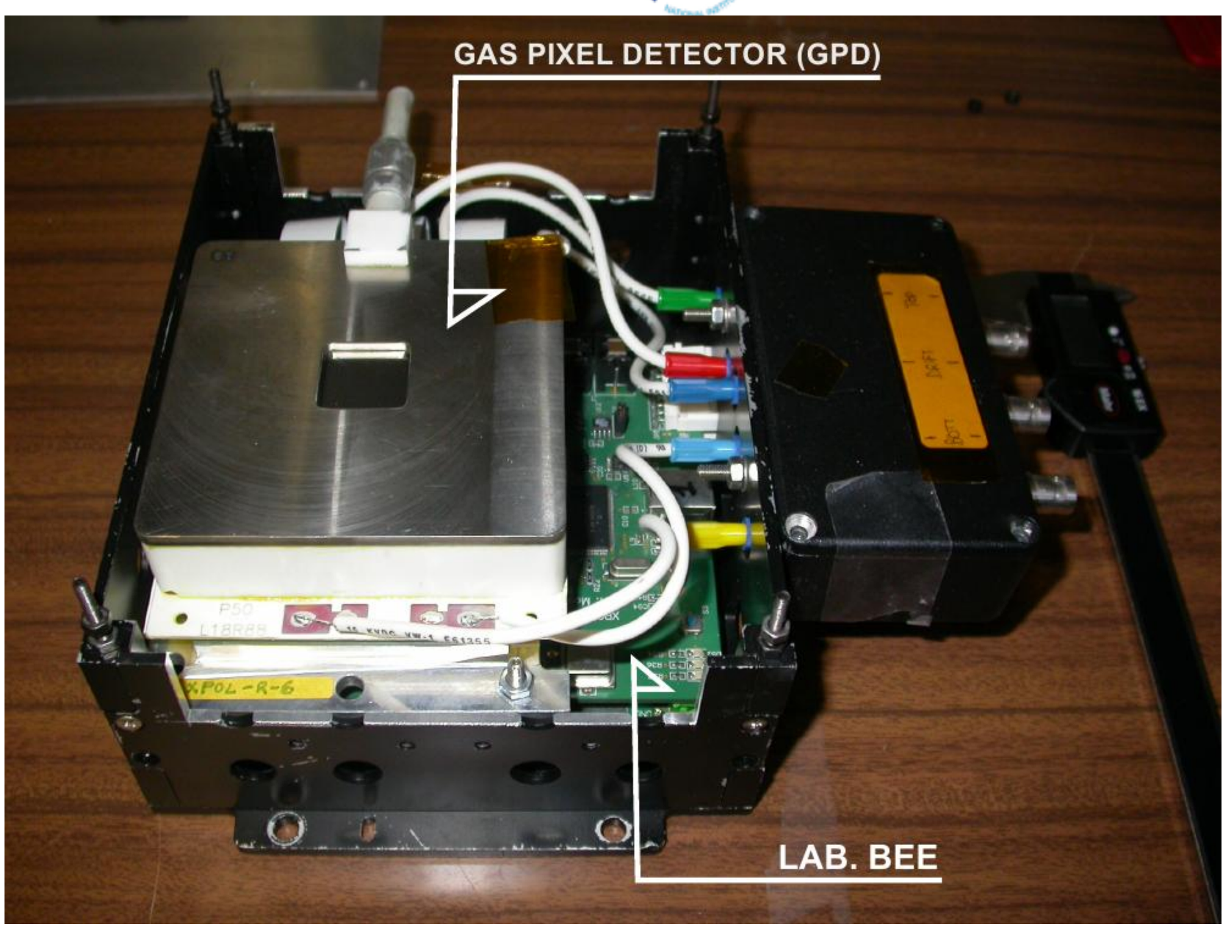

X-ray Polarimeter (**Polarization**)

Weight	**16 kg**
Power	**25 W**
Energy Range	**10-35keV(for non-thermal bremsstrahlung)**

Acceleration Mechanisms in Pulsar Wind Nebulae

Chandra image of the Crab showed that it has a complex structure that is typical of the so-called pulsar wind nebulae. In order to understand the role of the magnetic field in the production the observed emission it is necessary to perform imaging polarimetry of the nebula

The morphology of the Crab Nebula

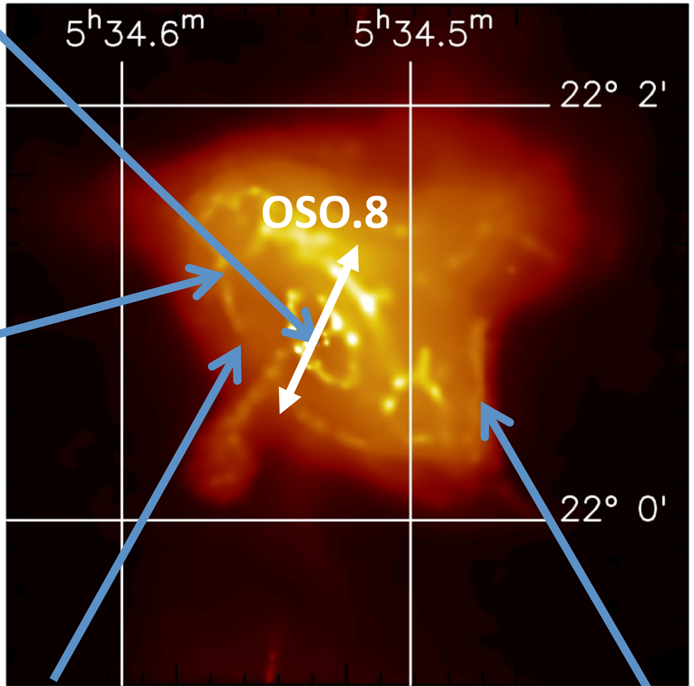

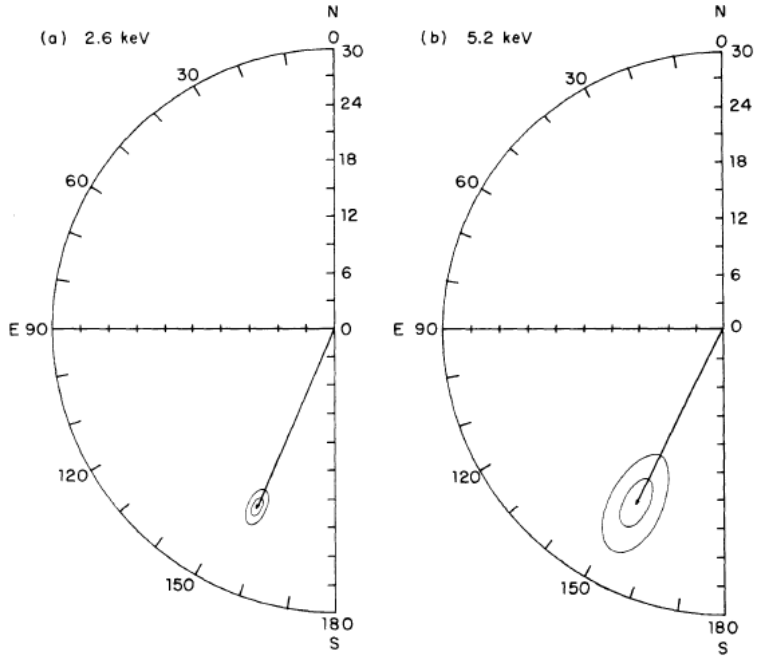

Measurement made by OSO-8

- The morphology of PWNs are complex.
- The OSO-8 integrated measure of the position angle is tilted with respect to jets and torus axis
- What is role of the magnetic field (turbulent or not ?) in accelerating particles and forming structures ?
- The measure of the pulsar polarization is facilitated.

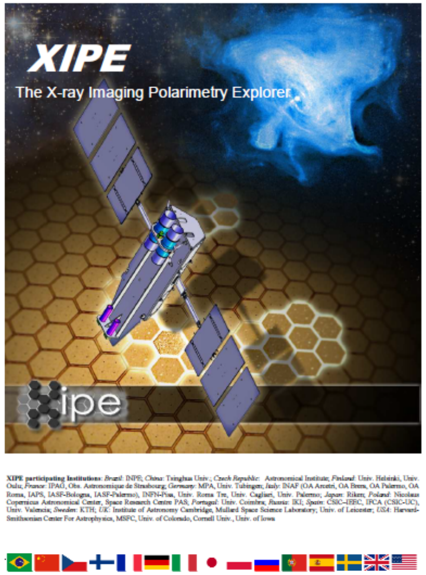

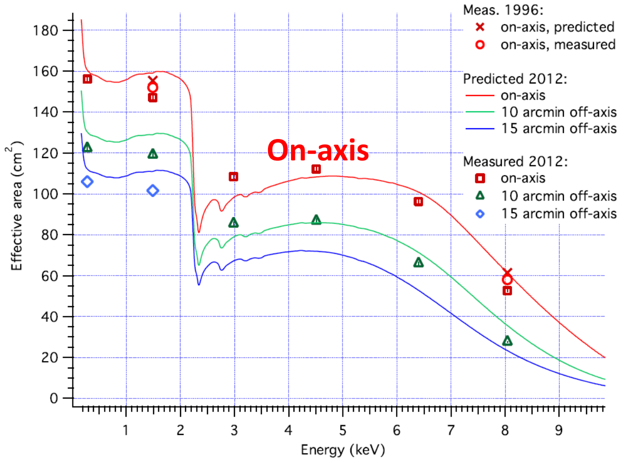

JET-X effective area (1 optics)

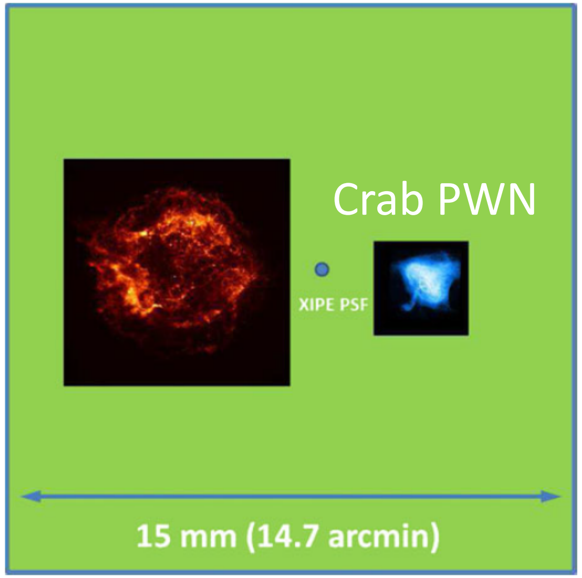

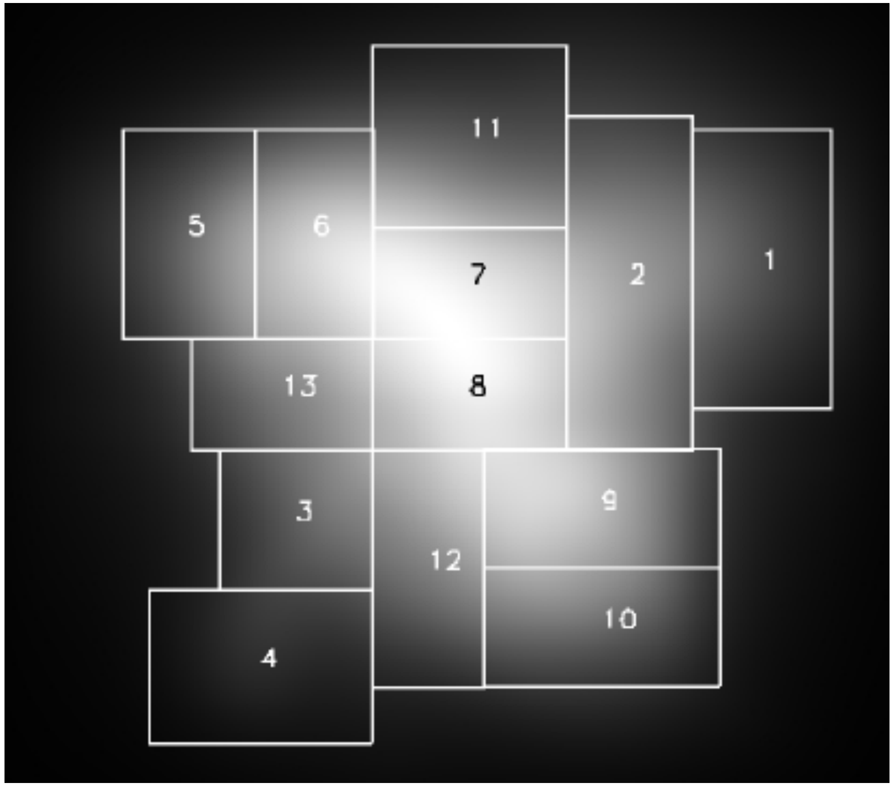

Region No.	$\sigma_{\rm degree}$ (%)	$\sigma_{\rm angle}$ (deg)	MPD (%)
1	0.7	1.1	2.2
2	0.5	0.8	1.5
3	0.8	1.3	2.5
4	1.0	1.6	3.2
5	0.7	1.1	2.2
6	0.5	0.9	1.7
7	0.5	0.8	1.6
8	0.5	0.8	1.6
9	0.5	0.9	1.7
10	0.7	1.1	2.2
11	0.6	1.0	1.9
12	0.6	1.0	1.9
13	0.7	1.1	2.2

Polarization assumed 19%. Observing time 100 ks *(Fabiani et al., 2014)*.

How many PWNs we can observe ?

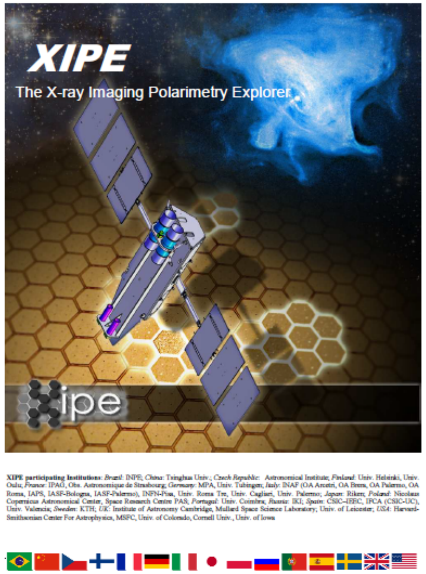

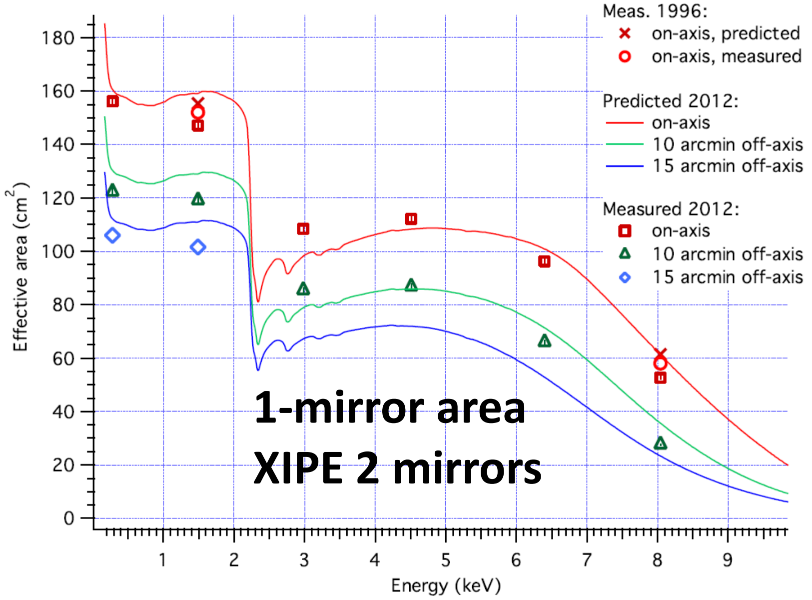

No.	Name	Distance (kpc)	Size (pc)	Size (arcmin)
2	Crab	2	1.2	2
7	Jellyfish	5	4.5	3
13	Vela	0.29	0.1	1.2
41	G0.9/G0.87+0.08	10	2.2	0.8
48	MSH1162/G291.020.11	1	1.1	3.8

From Kargaltsev, O.,&Pavlov, G. G. 2008

mCrab PWNs can be observed in 500 ks in 5 regions with an error on the angle of 10^{o}

Acceleration mechanisms in shell-like SuperNovae

Above 10 keV an extended power-law in the spectrum indicates the presence of a non-thermal component.
It is synchrotron emission (polarized) ?
Imaging Polarimetry can probe the emission mechanism in the energy range where lines are not present.

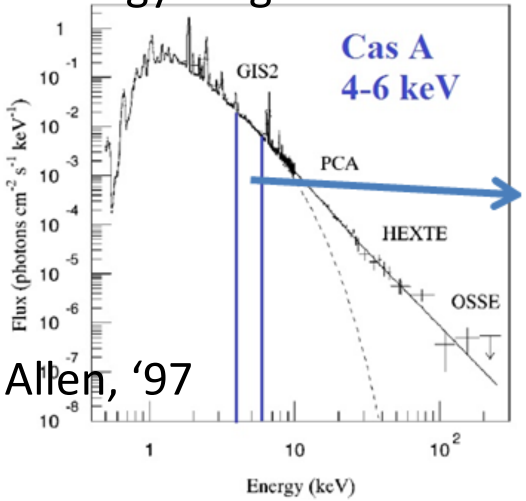

Allen, '97

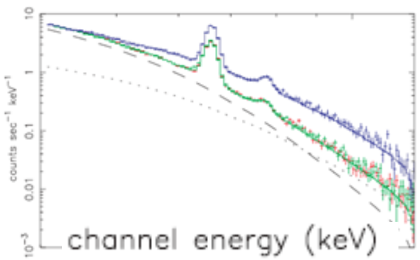

Bleeker et al., 2001.

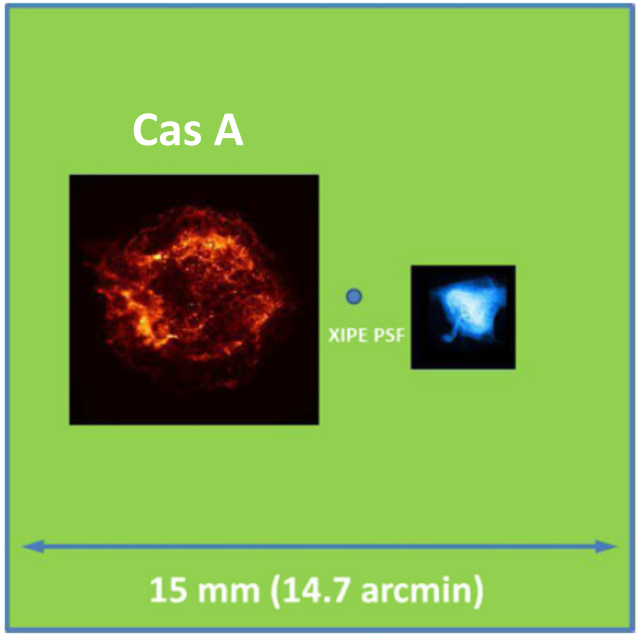

Region No.	σ_{degree} (%)	σ_{angle} (deg)	MPD (%)
1	2.4	6.6	7.7
2	2.7	8.3	8.8
3	2.1	5.9	6.7
4	2.9	7.8	9.5
5	1.9	5.3	6.1
6	3.5	11.0	11.1
7	3.6	11.0	11.6

T = 2 10^6 s

XIPE/GPD simulated image of Cas A (2-4) keV

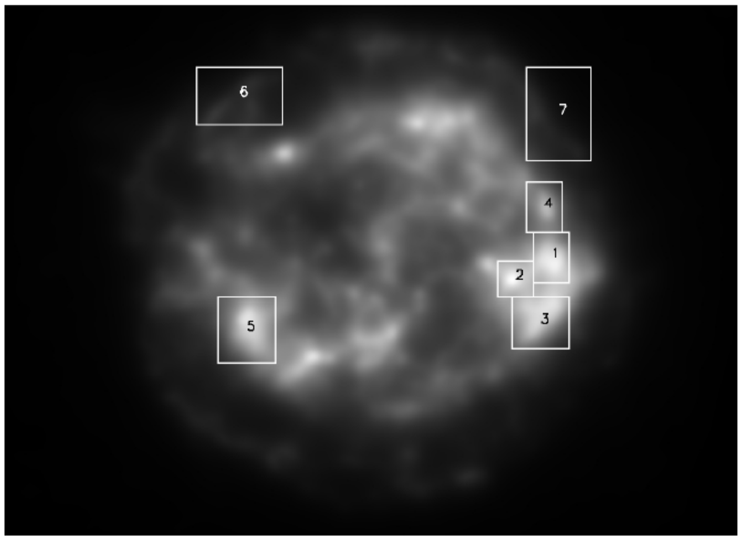

Fabiani et al., 2014

Since the power law is 22% of the total emission (4-6 keV angularly averaged, XMM data, Bleeker et al., 2001). Assuming P = 50 % of the non-thermal component, we expect P = 11 % for the observed radiation.

The role of synchrotron can be investigated by polarimetry making clear the role of the magnetic fields in generating the observed radiation.

How many Supernova Remnant can we observe ?

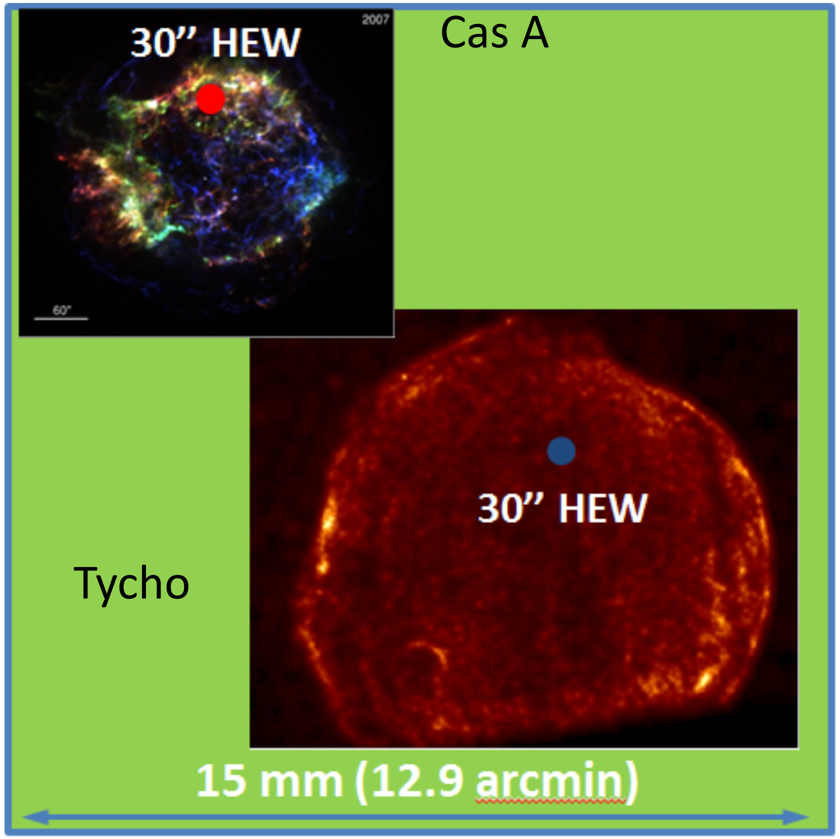

Field of view

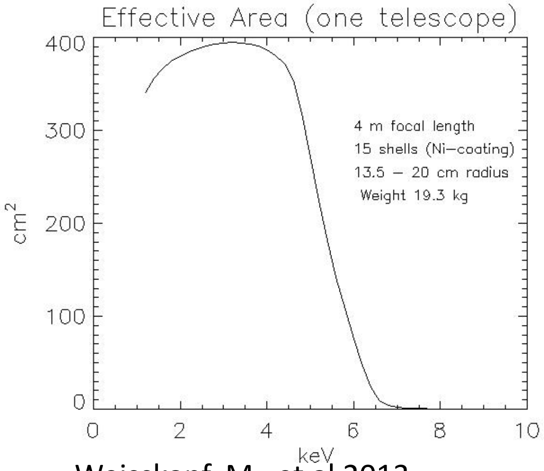

Weisskopf, M. et al 2013

Three of this optics with 30'' HEW.

MDP (4-6 keV) with T_{obs} = 10^5 s

Name	**Flux** (5 keV, ph/s/keV/cm^2)	**MDP** (4-6 keV)	Angular size (Approx.[53])
Cas A	$1.3\ 10^{-2}$	2.75%	4'
Kepler	$5.3\ 10^{-4}$	13.5%	4'
Kes 73	$5.5\ 10^{-4}$	13.3%	2.5'
W49 B	$5.6\ 10^{-4}$	13.3%	3'
W66	$1.5\ 10^{-4}$	25.7%	15'
Tycho	$3.3\ 10^{-3}$	5.5%	8'
IC 443	$1.5\ 10^{-3}$	8.1%	15' × 20'
MSH 11-54	$1.1\ 10^{-3}$	9.39%	8'
Kes 27	$1.4\ 10^{-4}$	26.4%	20'
RCW 103	$5.2\ 10^{-4}$	13.7%	15'

Cas A flux from Blecker 2001. Sizes from Seward, F. D., 1990.

- Example of *meaningful* observation when made angular resolved in **10^6 s but in 10 regions**.
- The power law is 22% of total emission (angularly averaged, Bleeker et al., 2001).
- Non thermal emission (synchrotron or bremsstrahlung) with respect to thermal bremsstrahlung
- The role and the morphology of the magnetic fields

Sgr B2 and other molecular Clouds in the Galactic Center region

See the talk of Frédéric Marin on Wednesday

SgrB2 is a giant molecular cloud at ~100pc projected distance from the Black Hole.

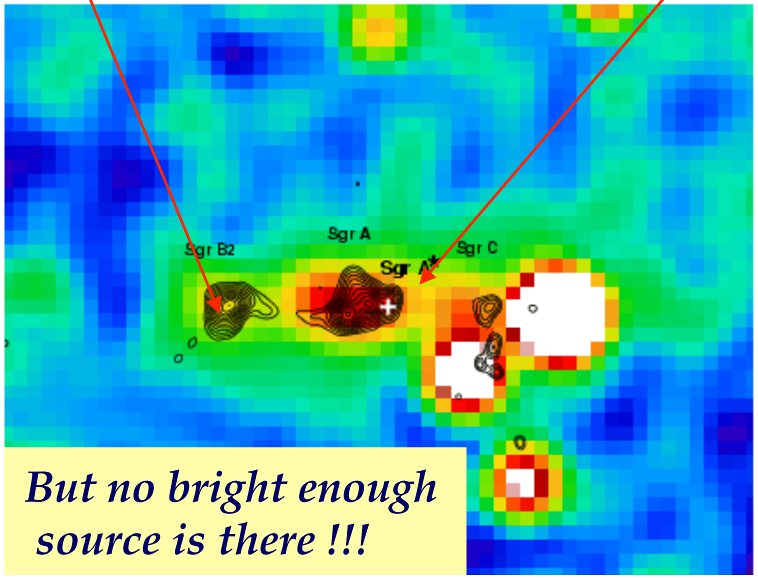

But no bright enough source is there !!!

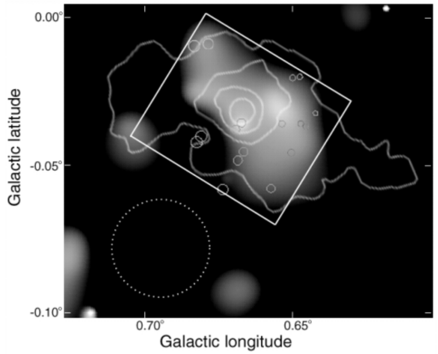

Chandra image.

Pure reflection spectrum (Sunyaev et al. 1993)

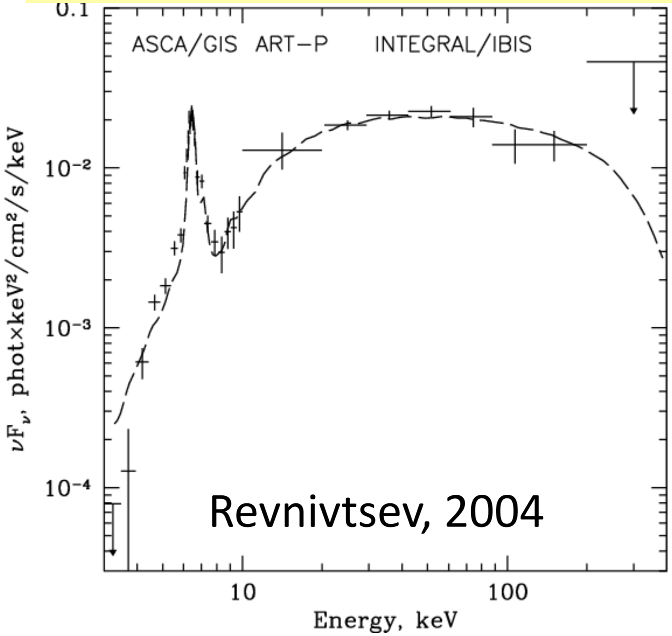

Revnivtsev, 2004

Is SgrB2 echoing past emission from the BH, which was therefore one million time more active ~300 years ago ??? (e.g. Koyama et al. 1996)

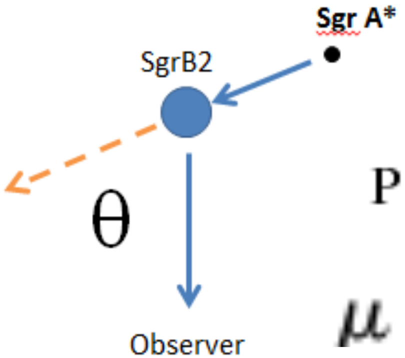

$$P = \frac{1-\mu^2}{1+\mu^2}$$

$$\mu = \cos\theta.$$

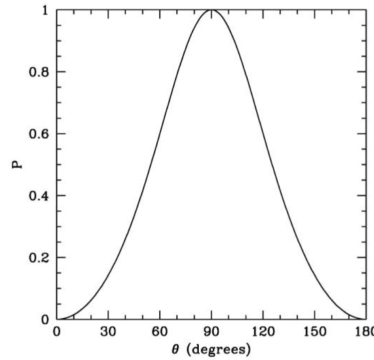

If Sgr B2 is reflecting radiation coming from SgrA* the observed radiation is polarized by scattering (Churazov 2002) pinpointing SgrA* and providing the real distance of the molecular clouds.

SGR B2 in the 2-10 keV energy band is a dim extended source.
What about the background?

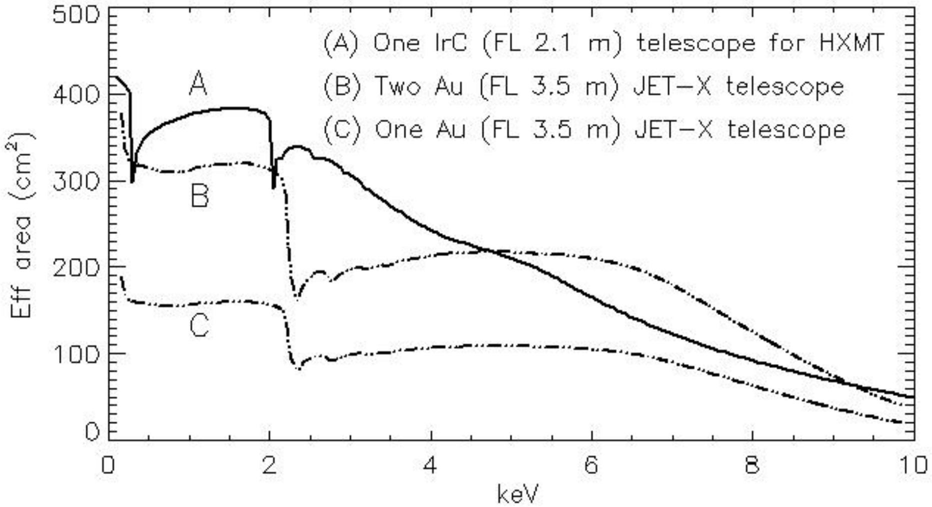

A => *XILPE for the next ESA-CAS S-mission*

B => *XIPE proposed at 1st call for an ESA S-mission*

NAME	Scattering Angle	P
*(**) Sgr B2	37.6 (80.5)	**22.9 % (94.2%)**

Polarization for a single scattering from SgrB2

(*) Reid 2009, (**) Ryu 2013

SGRB2 2-10 keV							
XIPE Crab rate 47 c/s (1 Mirror)	Focal Length	Rate 1 Mirror (c/s)	SGRB2 Area	Backg. (Ne, c/s) Optim.	Backg. (CH4) Pessim.	MDP ($2\ 10^6$ s) (**Opt.**/Pess.)	
	350 cm	4.1E-4	1.5 mm x 3.0 mm	**4.0E-5**	7.9E-4	**18**	31
XILPE Crab rate 95 c/s (1 Mirror)	Focal Length	Rate 1 Mirror (c/s)	SGRB2 Area	Backg. (Ne, c/s) Optim.	Backg. (CH4, c/s) Pessim.		
	210 cm	8.2E-4	0.92 mm x 1.9 mm	**1.4E-5**	2.8E-4	**18**	21

There are many molecular clouds around the galactic center !

117 arcmin; color code : **1-3 keV ; 3-5 keV; 5-8 keV**

36 arcmin

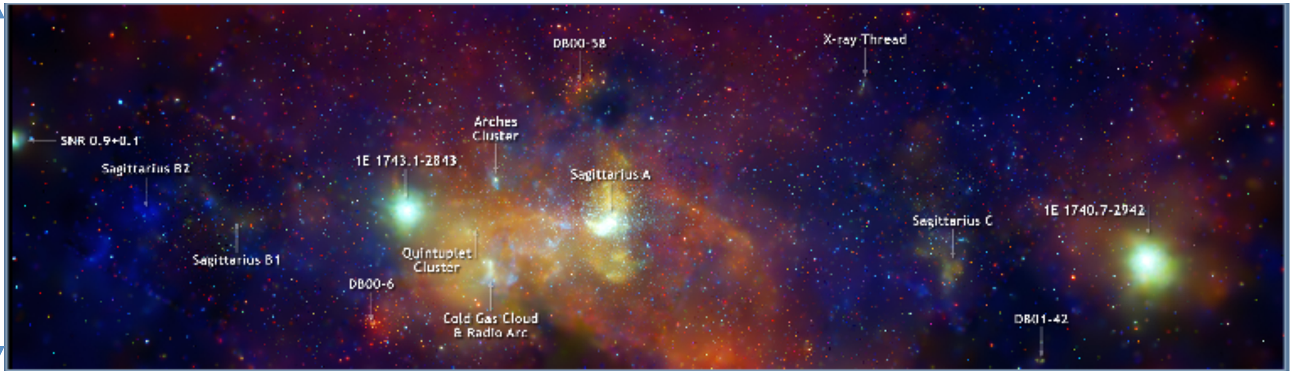

NAME	Scattering Angle	P	MDP (2-10 keV) XIPE (T=2 10^6s)	MDP (6-35 keV) NHXM (T = 5 10^5)
*(**) Sgr B2	37.6 (80.5)	**22.9 % (94.2%)**	18.2 %	4.3 %
**Sgr C1, C2, C3	136.3;48.8, 136.9	**31.3%; 39.5%; 30.5%**	12.0 %	12.0 %
***G0.11-0.11	124.2	**52.0 %**	8.4 %	9.7 %
***Bridge	163.3	**4.3 %**	12.0 %	10.2 %
***M1	166.5	**2.8 %**	19.9 %	13.2 %
***M2	158.2	**7.4 %**	23.9 %	18.4 %

Conclusions

- The Gas Pixel Detector shows already performances suitable for making sensitive astronomical X-ray polarimetry in space.
- Very good energy resolution and modulation factor are already stable in almost 3 years of ground operation.
- The sensitivity is only 1.7 times worse than GEMS/TPC for bright sources but it is not background limited even for the faintest sources accessible to polarimetry.
- Extension to higher energies allows for sensitive polarimetry of solar flares.
- Imaging allows for meaningful polarimetry of extended sources and crowded fields :
  PWNs, *SNRs* and *MCs* in the galactic center region.

Fine

X-ray polarization ‘*seen*’ by the GPD imaging

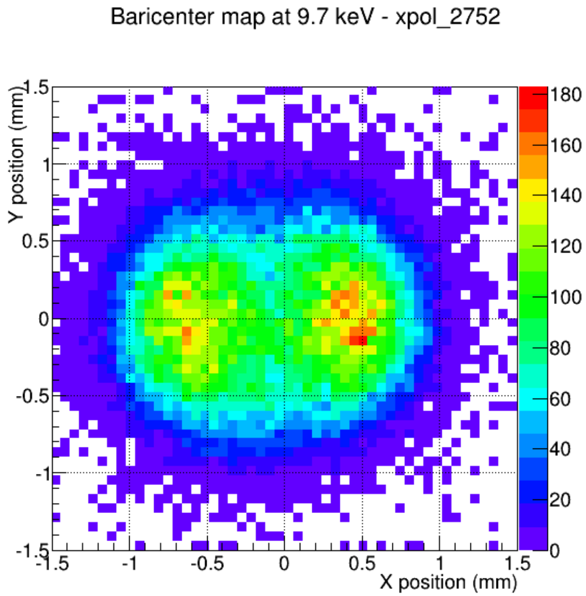

9.7 keV

Polarized

↔

E

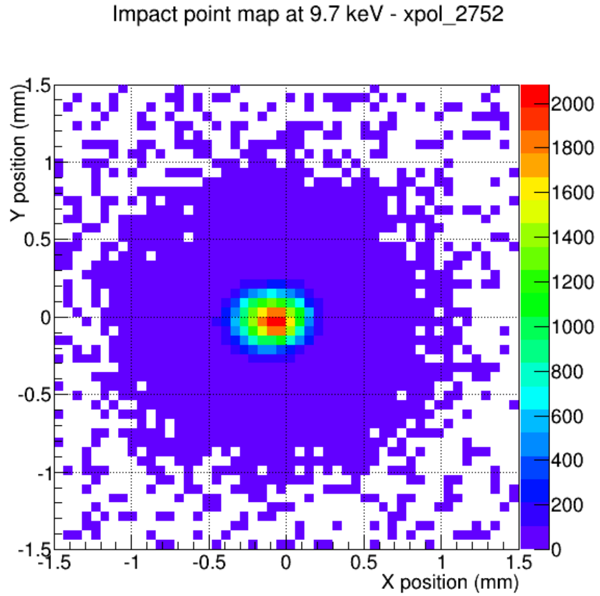

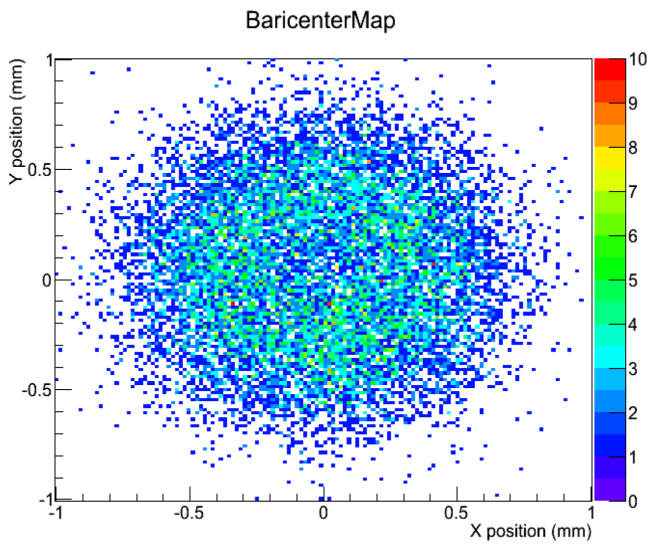

8 keV

Unpolarized

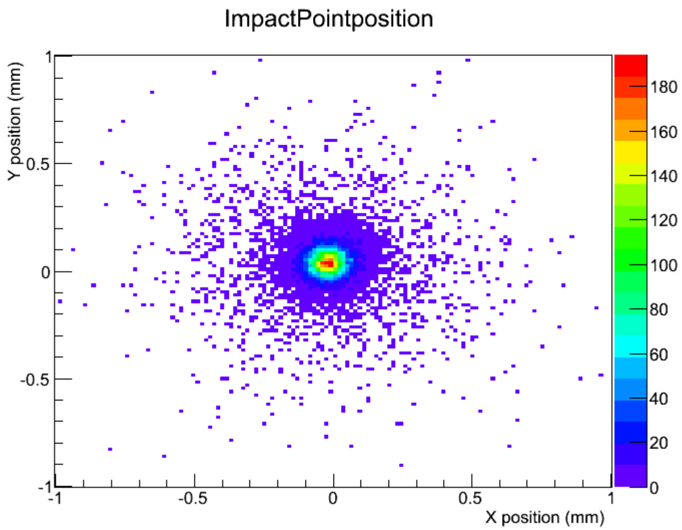

GPD-GEM90 Prototype

- The GPD-GEM90 design consists of 3 sub-components:

  - ✓ GPD-GEM90-Drift_assembly
  - ✓ GPD-GEM90-GEM_assembly

MEP-GEM90 prototype section:

  - ✓ GPD-GEM90-ASIC_Board_assembly

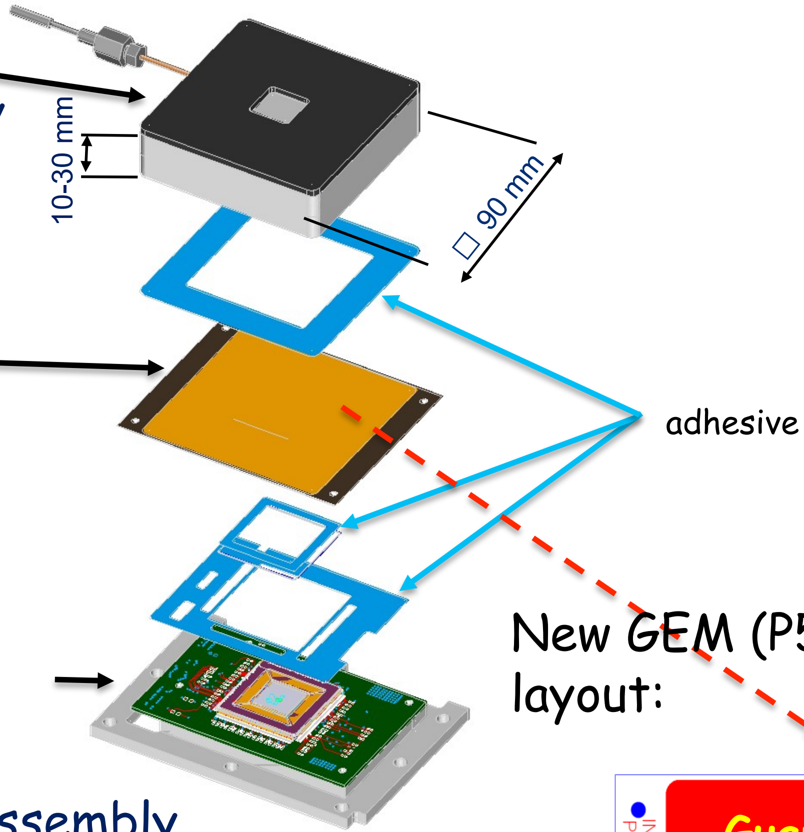

New GEM (P50L18R88) layout:

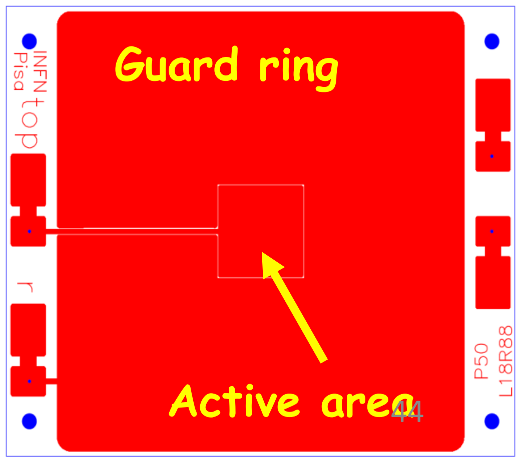

The GPD consists of three different assemblies glued together. The ASIC is in the KIOCERA ceramic package internally bonded. The KIOCERA is soldered and fixed to the board.

Quality Factor

What if we place the GPD at the focus of the (GEMS/TPC mirror) ?

$$MDP = \frac{4.29}{\int \mu(E) \times A(E) \times \varepsilon(E) \times F(E) dE} \times \sqrt{\frac{\int (A(E) \times \varepsilon(E) \times F(E) + \int (B_{diff}(E) + B_{res}(E))) dE}{T}}$$

QF is the scale factor of the MDP for a source dominated polarimeter.

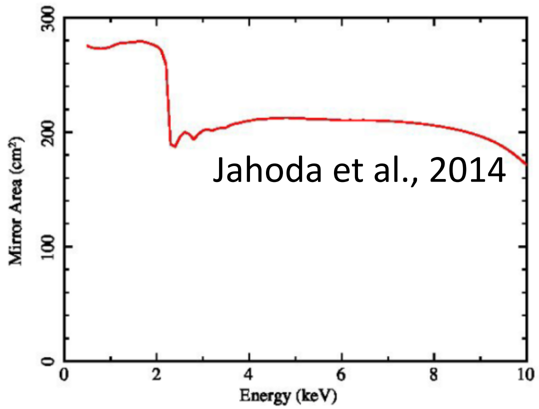

- The peak QF of GEMS/TPC is a factor 1.6 larger than the corresponding GPD.
- The GPD has a better response at lower energy.
- The GEMS/TPC ha a better response at higher energies.

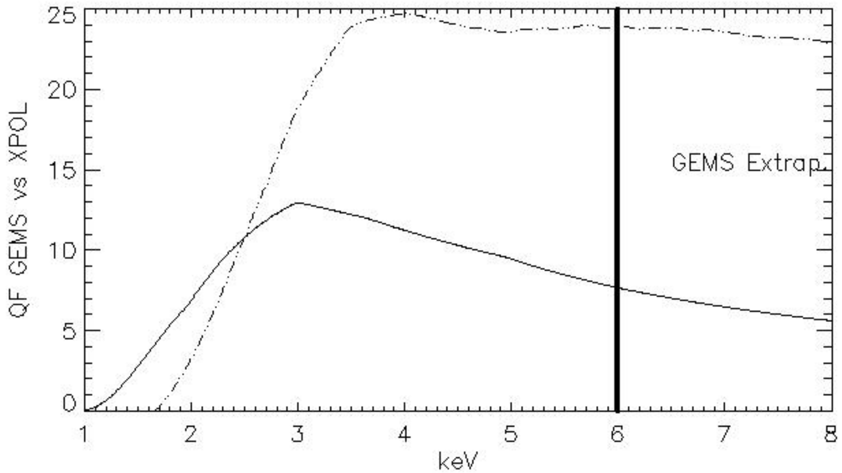

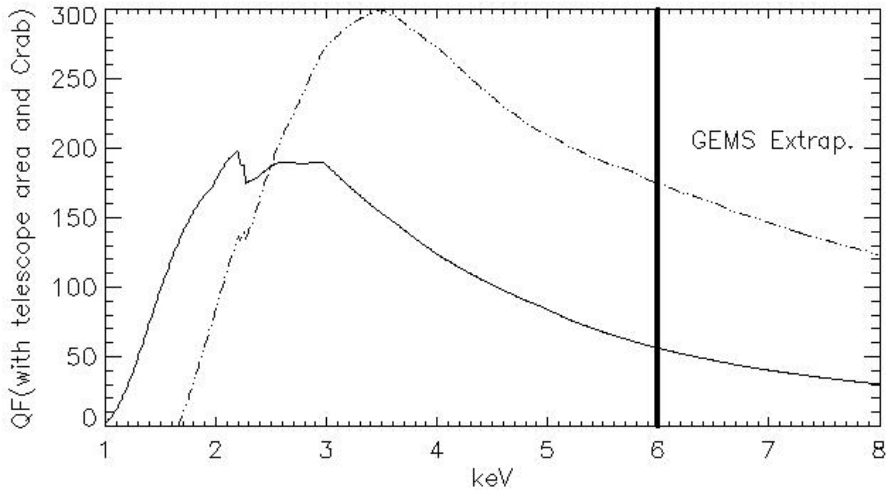

$$MDP \propto \frac{1}{\mu \cdot \sqrt{\epsilon}} = \frac{1}{QF}$$

$$\frac{1}{\mu \cdot \sqrt{\epsilon \cdot MirrorArea \cdot CrabSpectrum}} = \frac{1}{QF}$$

Sensitivity & Background

The sensitivity is a matter of photons but the 'limit' sensitivity could be a matter of background if imaging is not possible.

For example, if we consider the residual background of Wisconsin experiment on-board OSO-8 (Neon filled proportional counter and Methane filled proportional counter) we have the following :

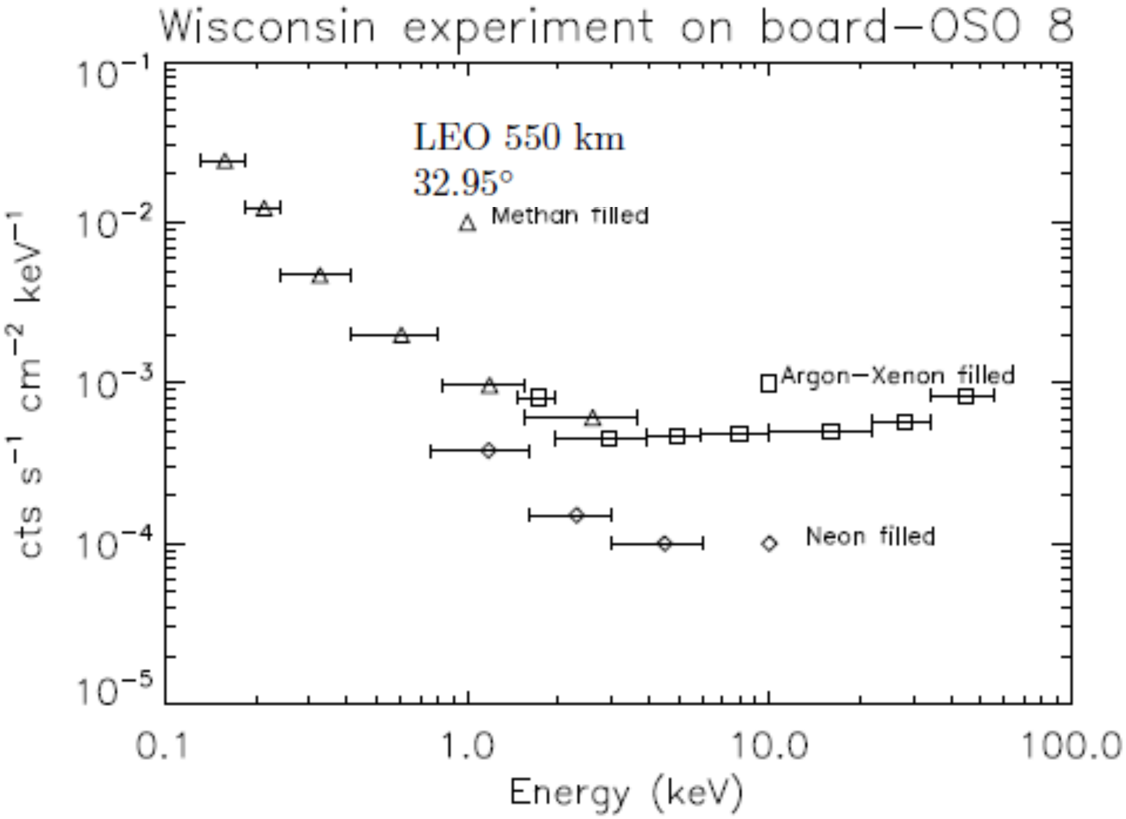

How the limit sensitivity depends on background.

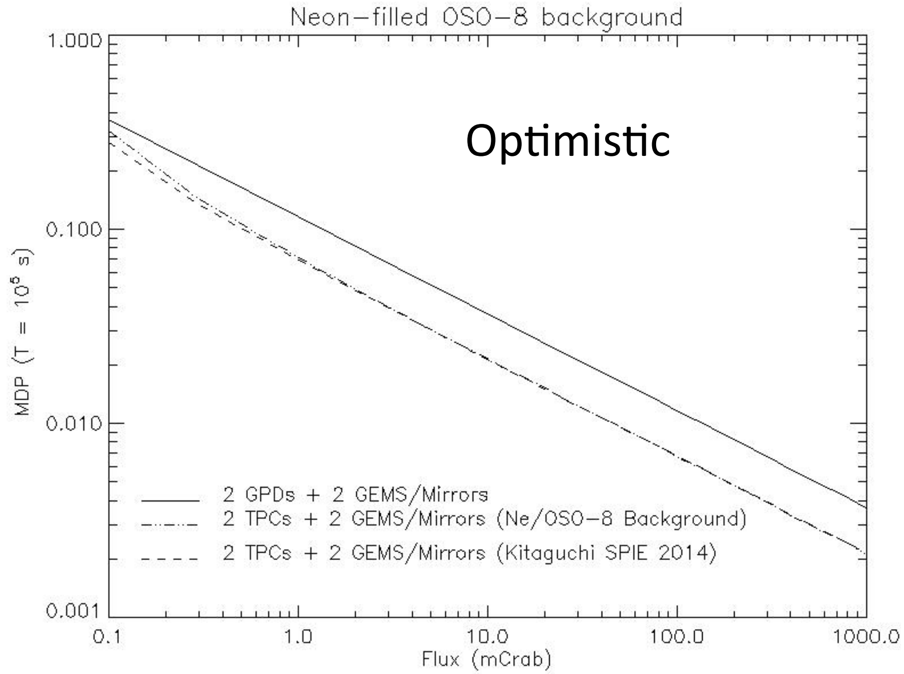

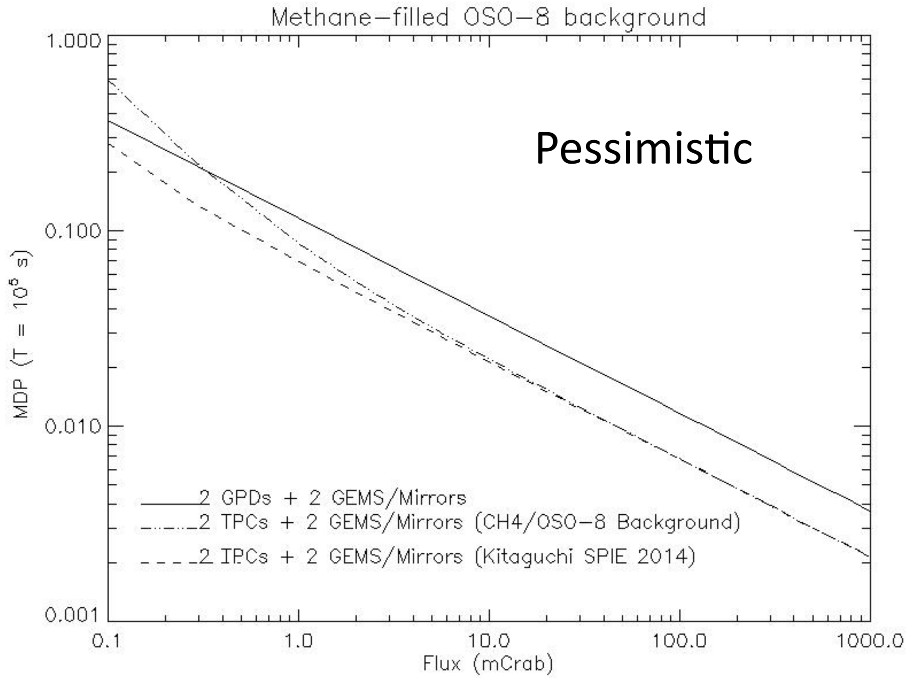

Residual background is larger if the sensitive area is larger :

GPD Area = 3.3 10^{-3} cm^2 (PSF = 30'', 4.5 m Focal lenght)

TPC Area = 1.5 cm x 31.2 cm = 46.8 cm^2

A mistake of a factor 10-20 in the background counting rate jeopardizes the polarization measurements below 5-10 mCrab for GEMS/TPC while GPD being imaging GPD is always source dominated down Fluxes << 1 mcrab :

What is the contribution to the modulation curve of the background ?

Other pictures@ PANTER

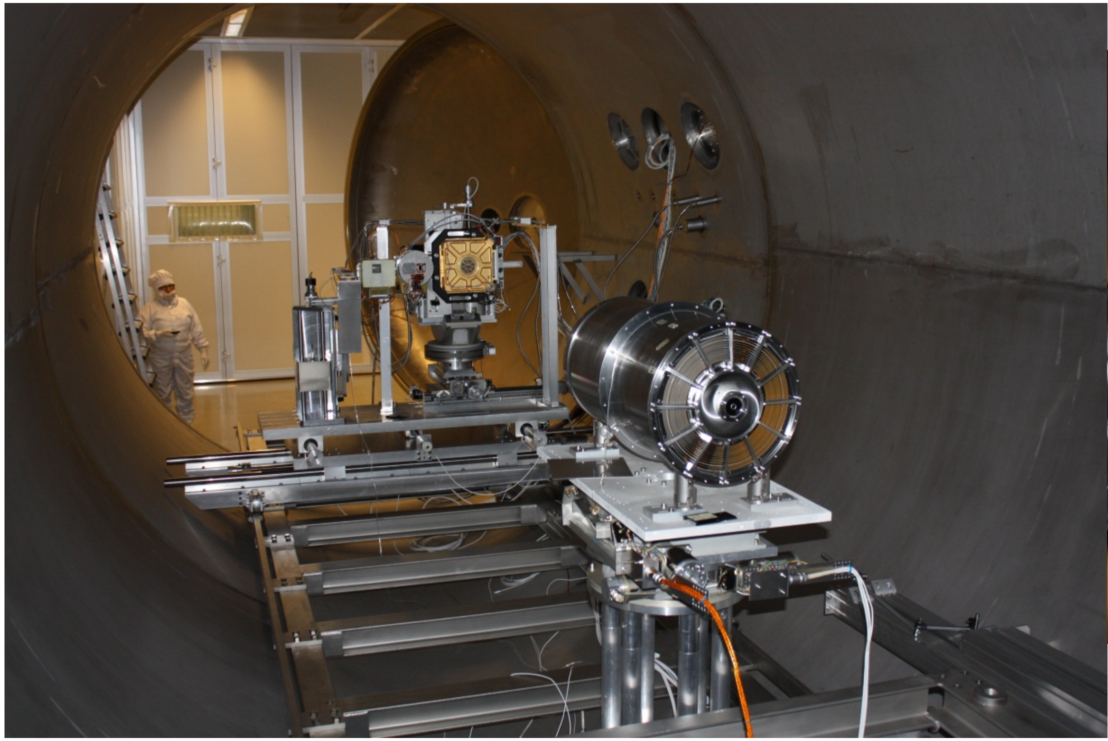

A high level of cleanness is required.

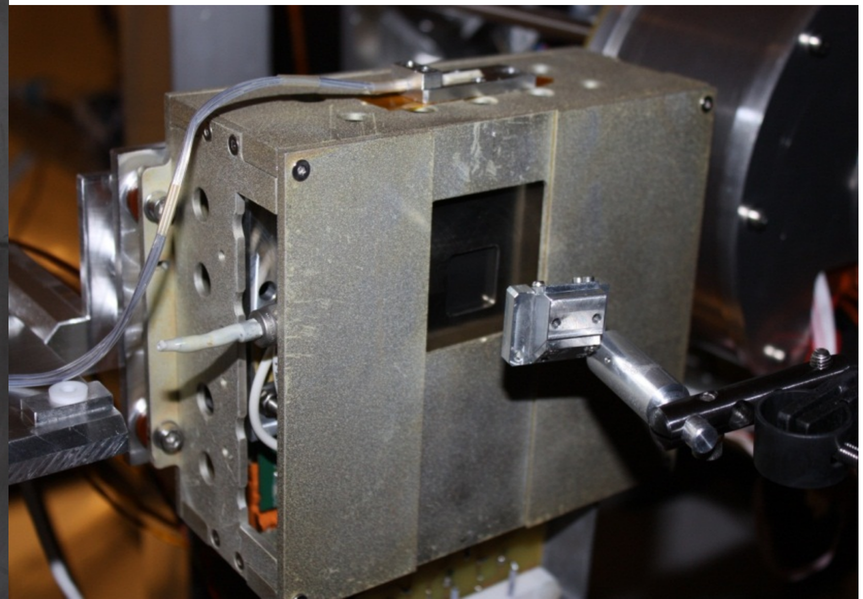

GPD in the PANTER chamber with a ^{55}Fe calibration source.

X and gamma missions devoted to solar physics and capable to image solar flares showed that the emission is localized in two foot-prints and in one loop top. This separation is evident at higher energy (> 20 keV) while at lower energies the emission is distributed along the fields lines.

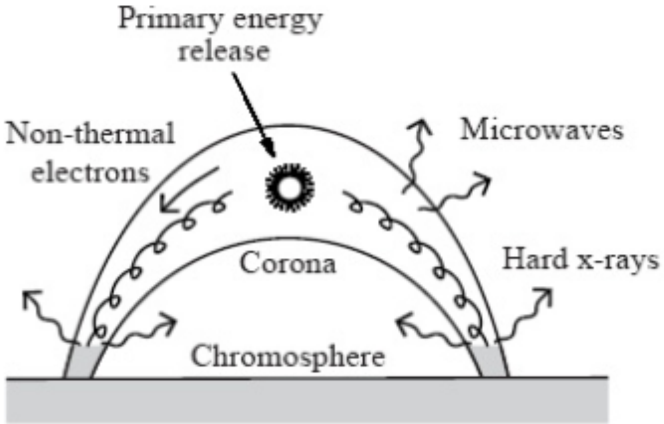

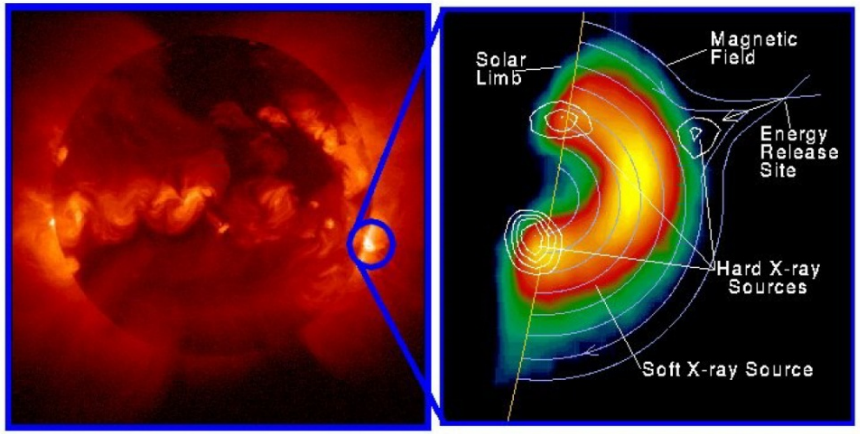

Yohkoh X-ray Image of a Solar Flare, Combined Image in Soft X-rays (left) and Soft X-rays with Hard X-ray Contours (right). Jan 13, 1992.

The morphology of a solar flare at hard X-rays is complex with a top source and two foot-prints.

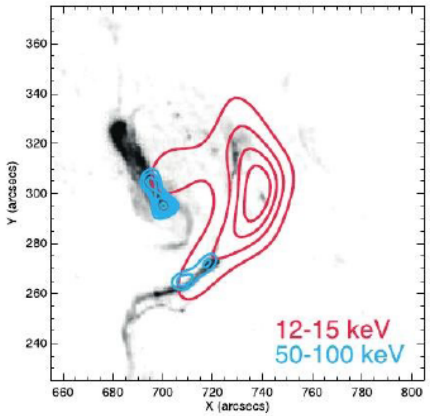

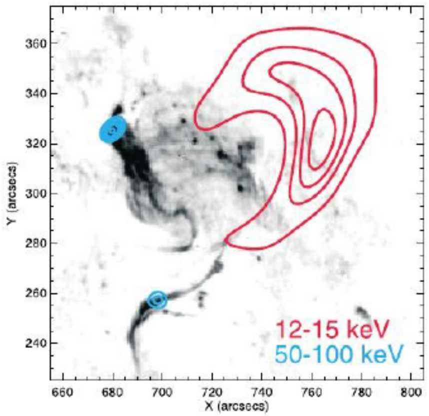

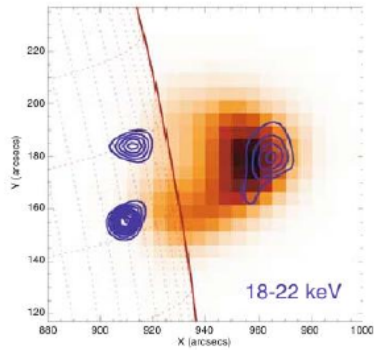

The angular separation between foot-points is of about 20''. Therefore, to make images, an angular resolution of at least 10''-20'' is needed to single out each source.

Beams of electrons produce non-thermal Bremsstrahlung which is polarized.

The X-ray flux above 10-15 keV is expected to be polarized providing a sensitive diagnostic of the electron beams generated from the magnetic reconnection event.

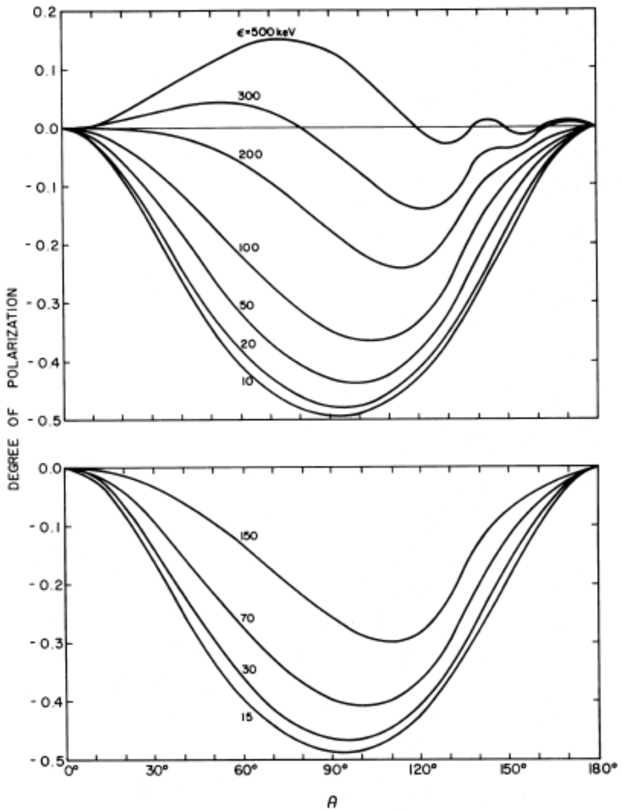

Bai and Ramaty, 1978

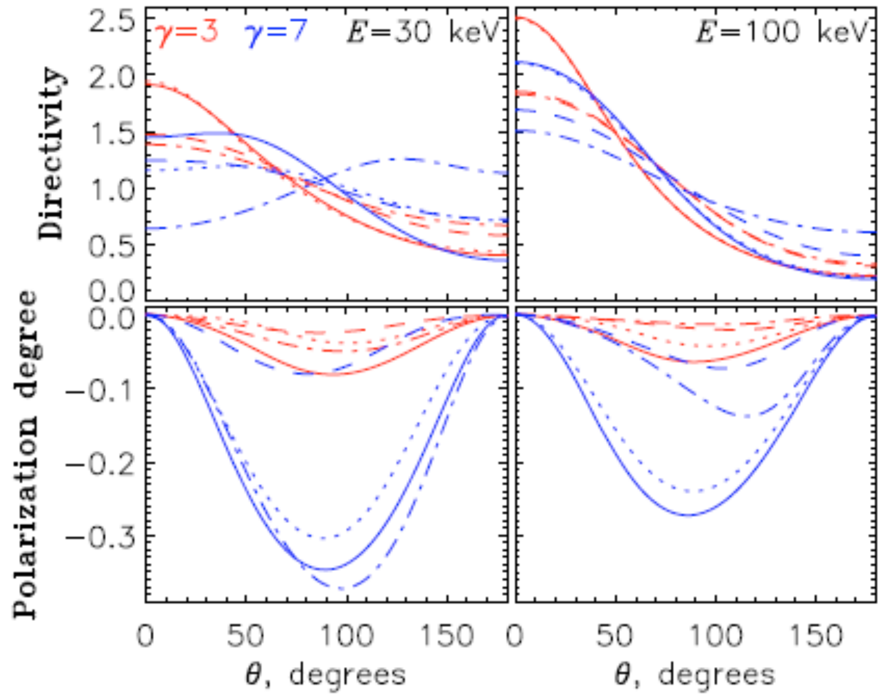

Zharkova et al., 2010

Degree of Polarization of primary hard X-rays due to accelerated electrons with a power-law energy distribution moving toward the photosphere with velocity uniformly distributed in a cone with 30° aperture. Negative values P is parallel to the normal plane or radiation plane (p_o **k**).

θ Is the angle between the radiation direction and normal to the sun on the onset-point.

The maximum polarization of about 40 % is when the flare appears on the source limb.

Summary of polarization results for the flares studied

Flare number (RHESSI)	2072301	3110221	4111002	5011710	5011911	5012005	5082502
Date	July 23, 2002	November 2, 2003	November 10, 2004	January 17, 2005	January 19, 2005	January 20, 2005	August 25, 2005
N_{tot}	7439 ± 86	34723 ± 186	3816 ± 62	2142 ± 46	5688 ± 75	43313 ± 208	6139 ± 78
N_{acc}	2269 ± 10	21427 ± 31	506 ± 5	473 ± 5	783 ± 6	26907 ± 35	602 ± 5
N_{bg}	1758 ± 42	5135 ± 72	2047 ± 45	733 ± 27	2784 ± 53	5808 ± 77	3717 ± 61
N_C	3411 ± 97	8160 ± 202	1262 ± 77	937 ± 54	2121 ± 92	10598 ± 225	1820 ± 100
μ_{100} (%)	33.0 ± 1.6	32.4 ± 1.8	32.9 ± 1.7	33.4 ± 1.9	31.6 ± 1.5	34.4 ± 1.6	34.4 ± 1.6
μ_p (%)	0.6 ± 4.5	9.1 ± 3.9	11.7 ± 8.6	9.4 ± 8.2	17.1 ± 6.5	7.2 ± 3.3	2.2 ± 8.4
ϕ (deg)	151 ± 195	96 ± 12	104 ± 24	71 ± 29	170 ± 11	66 ± 14	102 ± 104
Π (%)	2 ± 14	28 ± 12	36 ± 26	28 ± 25	54 ± 21	21 ± 10	6 ± 25

Note. μ_p is the observed modulation factor. Π is the polarization degree of the flare, and ϕ its polarization angle given in heliocentric coordinates.

Errors are 1σ; E. Suarez-Garcia et al., 2006

Hard- X ray polarimetry from the mission RHESSI (100-350 keV) shows inconclusive results.

SPR-N scattering polarimeter (with one Beryllium scatterer and 6 CsI(Na) absorbers) on-board CORONAS-F satellite detected 90 solar flares from 2001 to 2005. For 25 events, an upper limit between 8% and 40% was determined. For one flare 29 October 2003 a polarization larger than 50 -70 % was detected (Zhitnik 2006) above 20 keV.

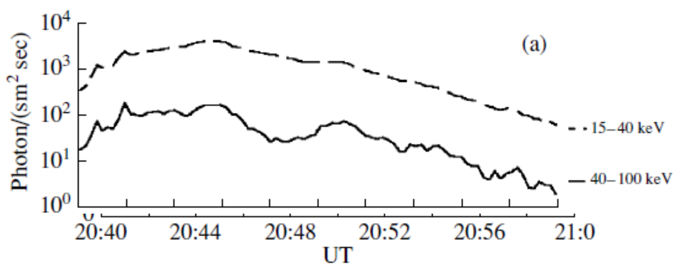

Zhitnik et al., 2006

29 Oct 2003, X10 Flare

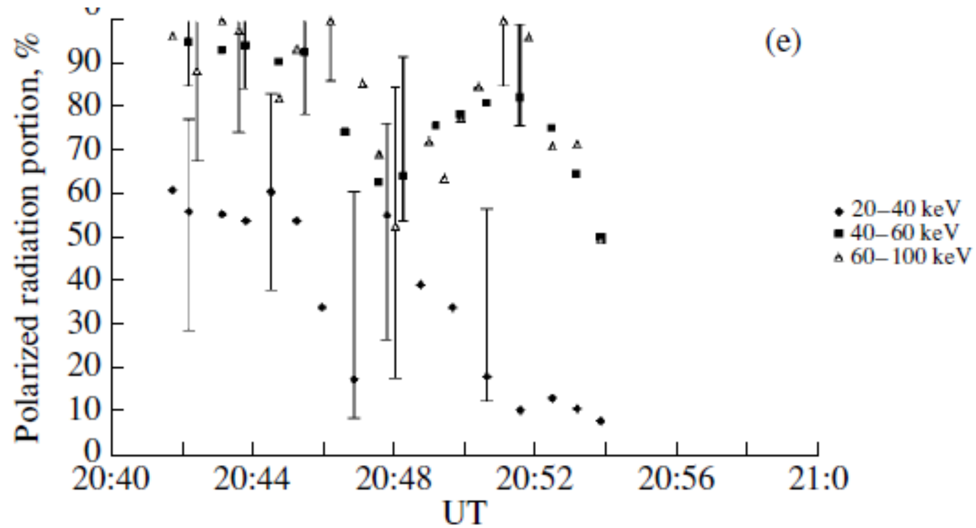

An example for X-ray polarimetry to probe the absolute positions of the molecular clouds in the Sgr A complex and solve the Sgr A* light-curve.

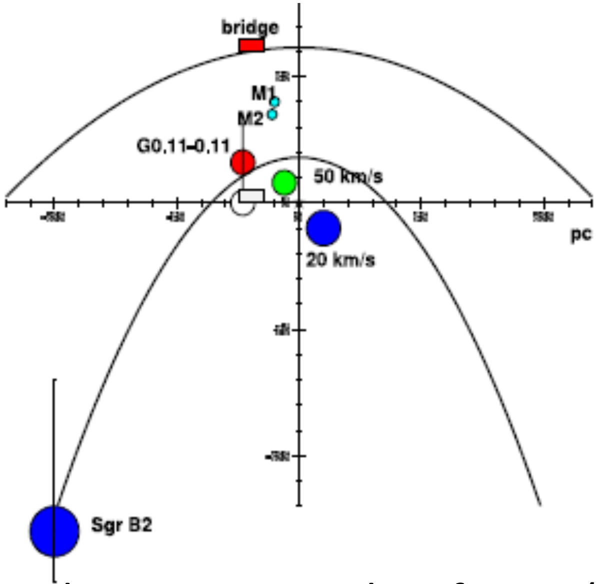

Sgr B2 is wide about 3' smaller than NHXM and Athena+ field of view.

Sgr C Complex is 15'x 12' wide smaller than the XIPE field of view. It can be observed with a single pointing.

Sgr A complex is wide about 8'x8' smaller than XIPE field of view. It can be observed with a single pointing

Absolute position taken from : (*) Reid 2009, (**) Ryu 2013, (***) Ponti 2012

NAME	Scattering Angle	P	MDP (2-10 keV) XIPE (T=2 10^6s)	MDP (6-35 keV) NHXM (T = 5 10^5)
*(**) Sgr B2	37.6 (80.5)	**22.9 % (94.2%)**	18.2 %	4.3 %
**Sgr C1, C2, C3	136.3;48.8, 136.9	**31.3%; 39.5%; 30.5%**	12.0 %	12.0 %
***G0.11-0.11	124.2	**52.0 %**	8.4 %	9.7 %
***Bridge	163.3	**4.3 %**	12.0 %	10.2 %
***M1	166.5	**2.8 %**	19.9 %	13.2 %
***M2	158.2	**7.4 %**	23.9 %	18.4 %

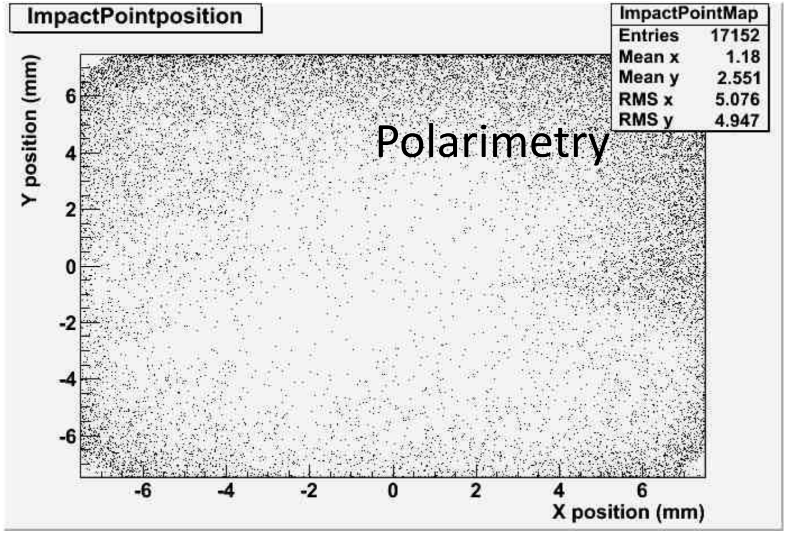

OLD DESIGN. Walls close to the ASIC

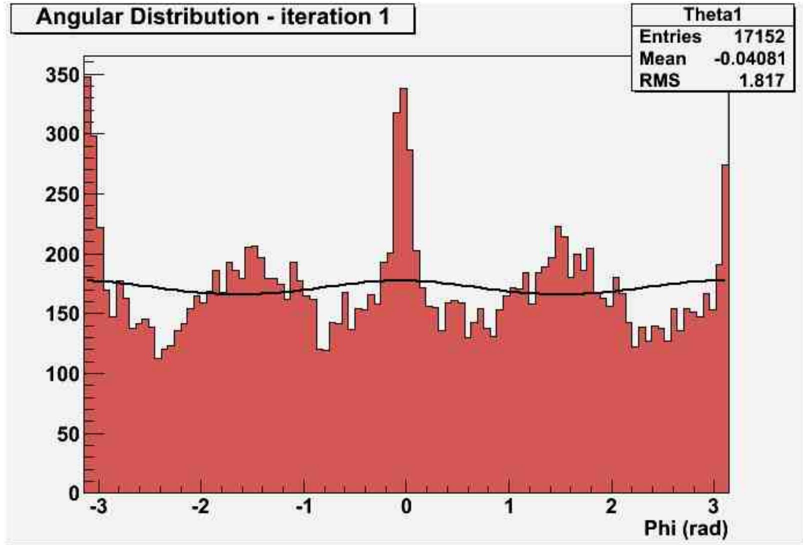

Environ. background spatial distribution of a GPD 2-cm; 2-bar filled with an ArDME gas mixture.

Modulation curve of the background that suggests that most of the background comes from the walls.

NEW DESIGN. Walls far from the ASIC edge.

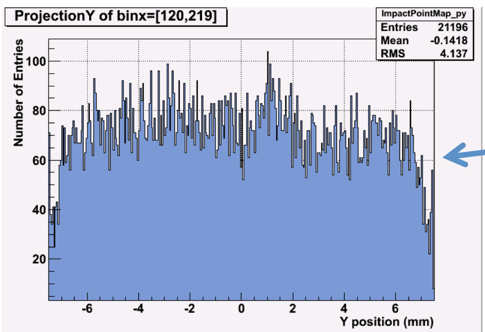

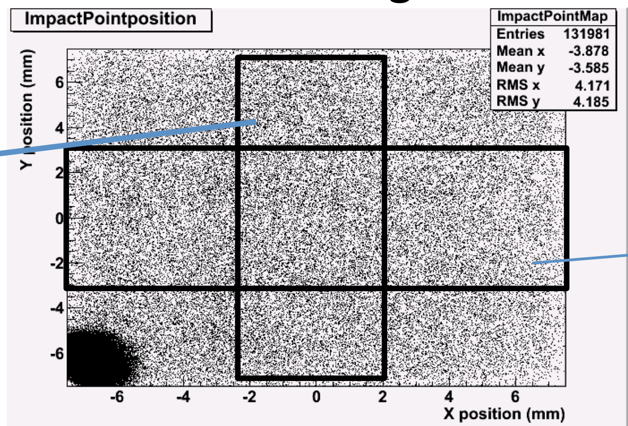

Projection on X of a slice excluding Fe^{55}.

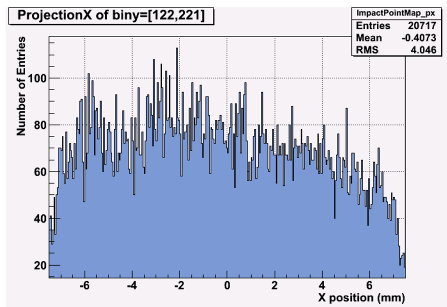

Projection on Y of a slice excluding Fe^{55}.

He-DME filled GPD with the new design. The Fe^{55} collimated source on the corner allows for preventing time-out of the electronics.

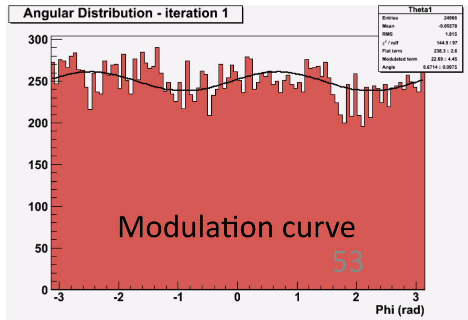

The payload

Size	**362×349×172.5mm**
Weight	**20.5 kg**
Power	**20 W**
Energy Range	**>10keV**
Energy Resolution	**3%@662keV**
Temporal Resolution	**1s(quiescent),32ms (flare-mode)**

Light-curves/Spectra
MPO/China

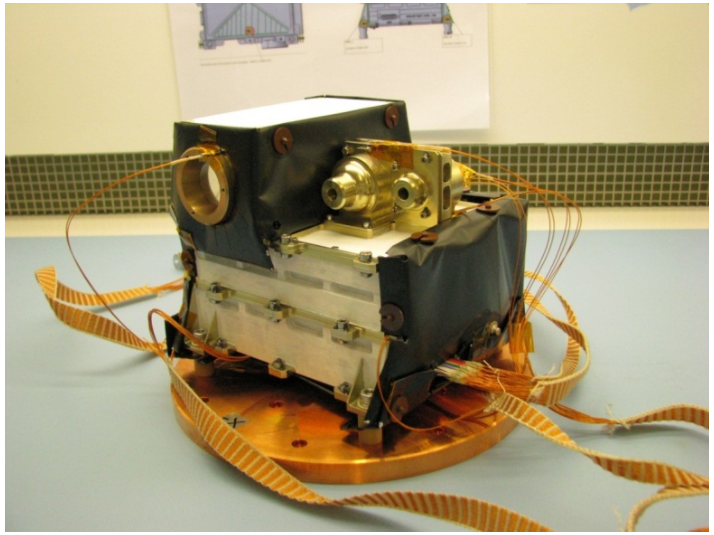

Mass	**2.5 kg**
Power	**5 W**
Energy Range	**Electrons: 20 keV – 30 MeV** **Protons: 20 keV – 100 MeV** **Heavy ions: ~10 MeV/nuc – ~200 MeV/nuc (species dependent)**
Time Resolution	**10s (species dependent)**

Particle transport
Cau Kiel/Germany

GEMS/TPC Background

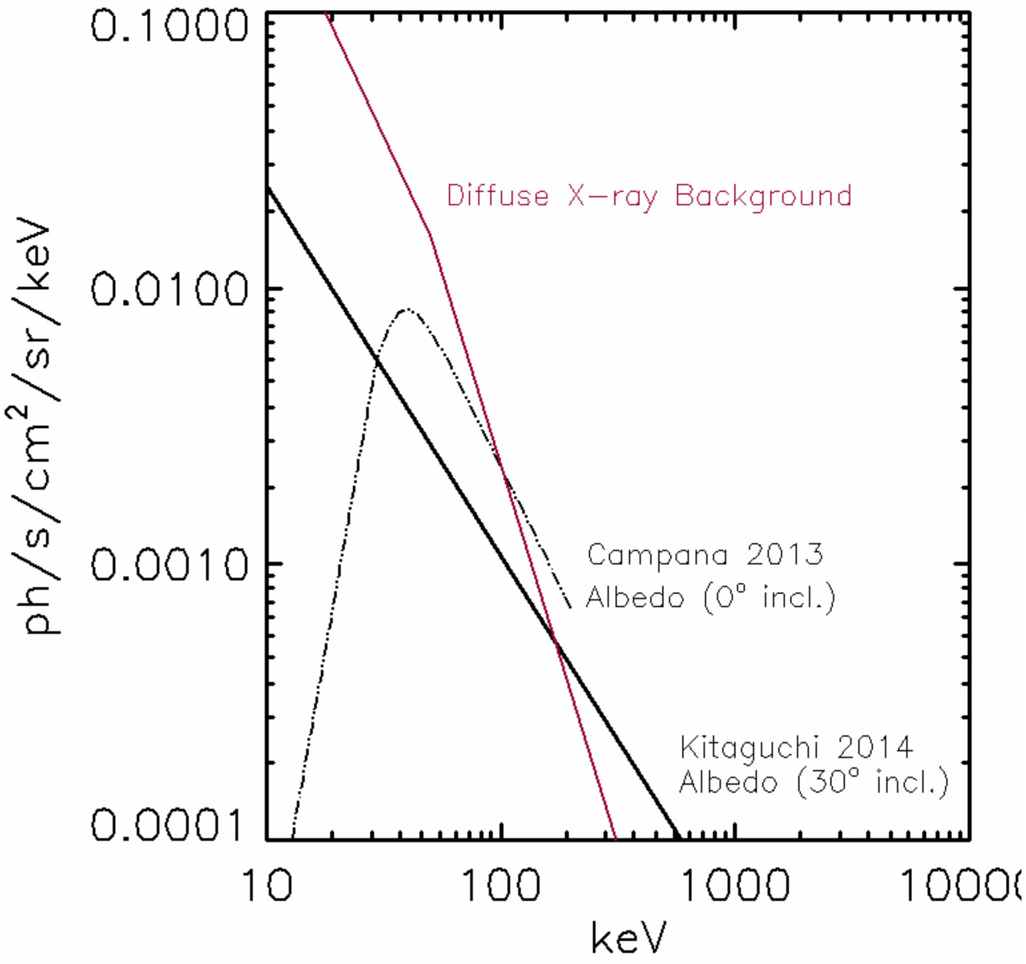

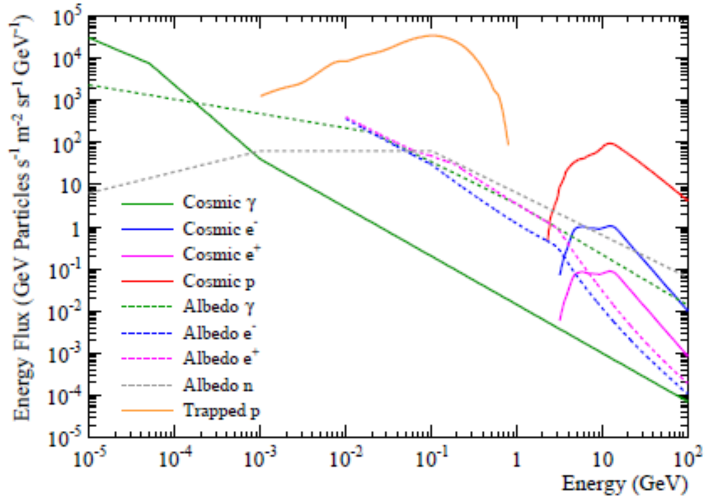

Figure 6. Orbit-averaged energy spectra of cosmic radiation input to the polarimeter background simulation.

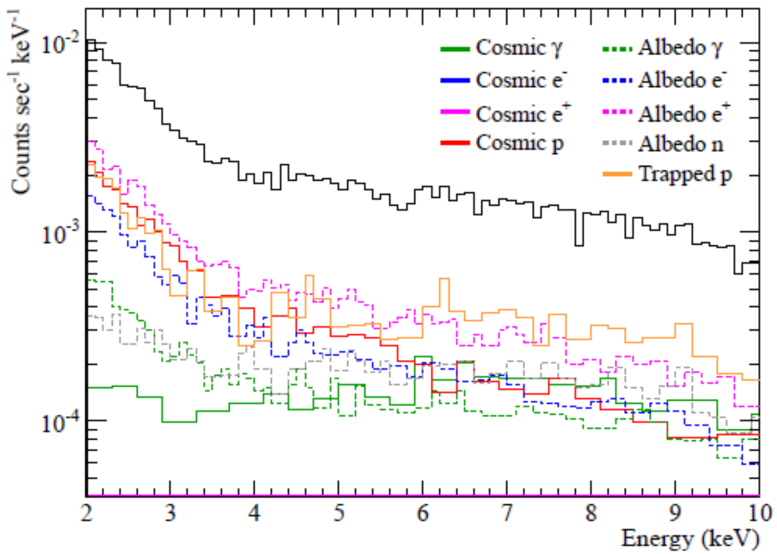

Kitaguchi et al., 2014

Was the GC an AGN a few hundreds years ago?

X-ray polarimetry can definitively proof or reject this hypothesis.

SgrB2 should be highly polarized with the electric vector perpendicular to the line connecting the two sources.

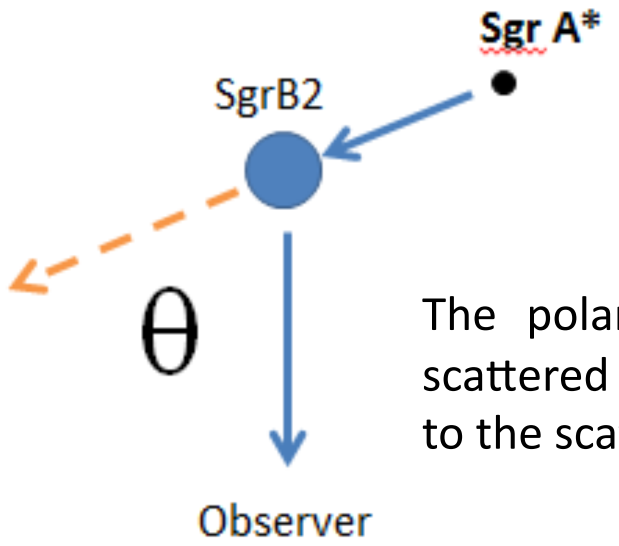

$$P = \frac{1 - \mu^2}{1 + \mu^2}$$

$$\mu = \cos\theta.$$

The polarization direction of the scattered radiation is **perpendicular** to the scattering plane.

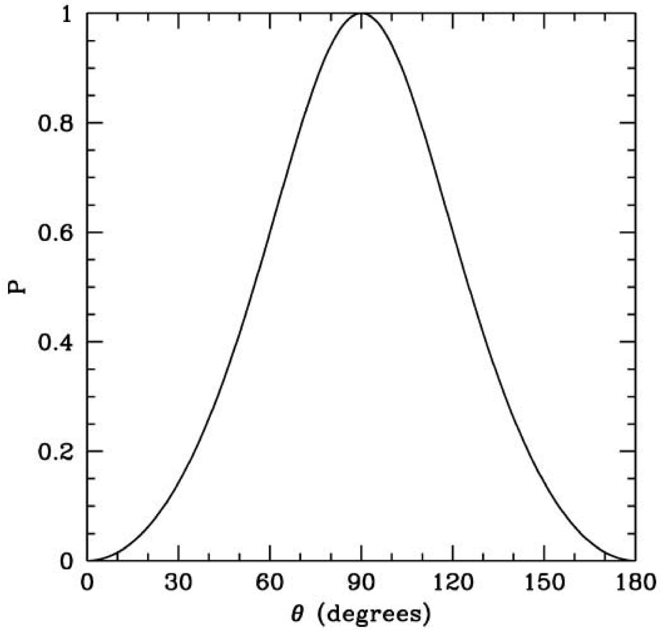

The degree of polarization would measure the angle and provide a full 3-d representation of the clouds (Churazov et al. 2002)

Quality Factor

What if we place the GPD at the focus of the (GEMS/TPC mirror) ?

$$MDP = \frac{4.29}{\int \mu(E) \times A(E) \times \varepsilon(E) \times F(E) dE} \times \sqrt{\frac{\int (A(E) \times \varepsilon(E) \times F(E) + \int (B_{diff}(E) + B_{res}(E)))dE}{T}}$$

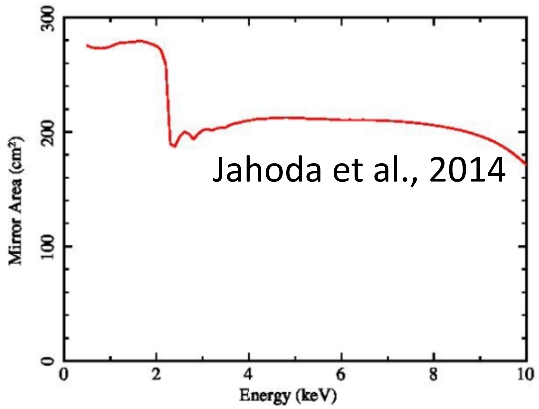

QF is the scale factor of the MDP for a source dominated polarimeter.

- The peak QF of GEMS/TPC is a factor 1.6 larger than the corresponding GPD.
- The GPD has a better response at lower energy.
- The GEMS/TPC ha a better response at higher energies.

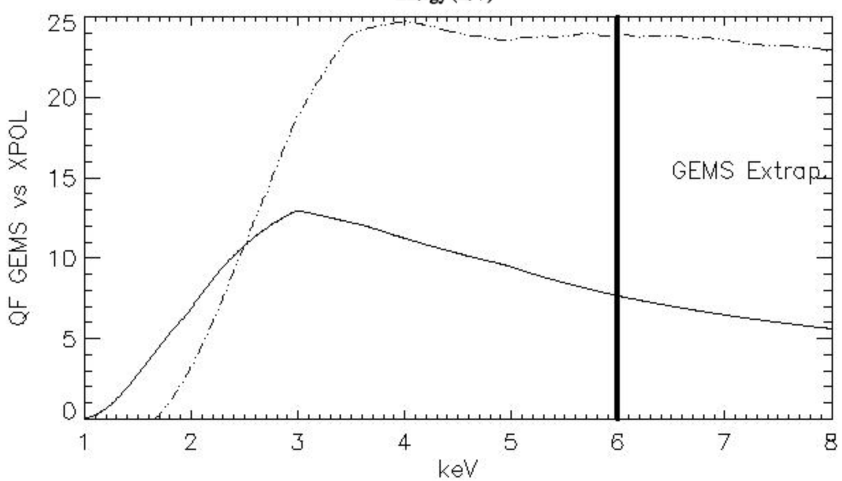

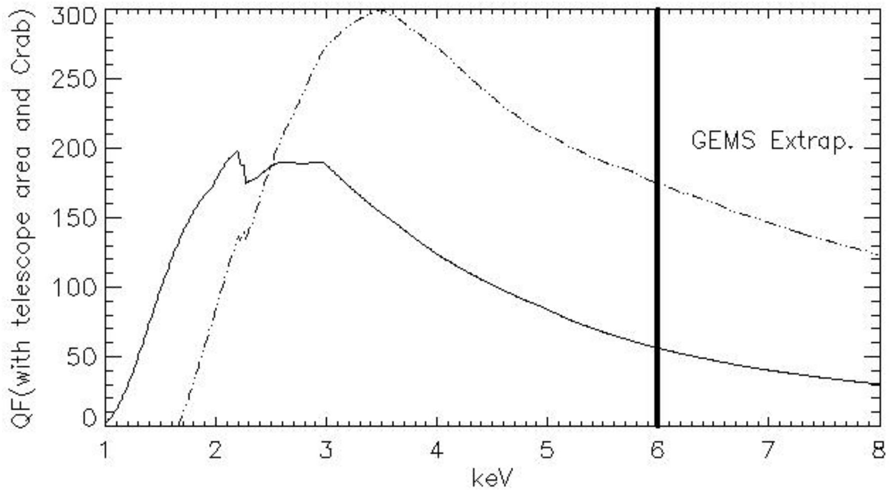

$$MDP \propto \frac{1}{\mu \cdot \sqrt{\epsilon}} = \frac{1}{QF}$$

$$\frac{1}{\mu \cdot \sqrt{\epsilon \cdot MirrorArea \cdot CrabSpectrum}} = \frac{1}{QF}$$